



Low-frequency characteristics of wave group–forced vortices

Joseph W. Long¹ and H. Tuba Özkan-Haller¹

Received 1 May 2008; revised 25 March 2009; accepted 20 May 2009; published 8 August 2009.

[1] The dynamics of vorticity motions forced by wave groups incident on an alongshore-uniform barred beach are analyzed. For both normally and obliquely incident wave groups, the potential vorticity and enstrophy equations reveal that the temporal variability of wave group–forced vortices is directly linked to the variability in the incoming wave groups rather than bottom friction, as previously hypothesized. Analysis of the lifespan of individual vortices further shows that the wave group forcing is responsible for not only the temporal variations of the vortices but also their eventual demise. Vortices in the simulations persist for 5 to 45 min, which is consistent with recent field observations. For oblique wave groups, the resulting vortices are advected by the mean current, yielding a signature in the frequency–wave number spectrum that is similar to that usually attributed to shear instabilities of the alongshore current. These results may explain previous observations of alongshore-propagating vorticity motions in the presence of a stable alongshore current. For simulations involving an unstable alongshore current, we find that the inclusion of wave group forcing results in velocity spectra that are much broader compared to the simulations that neglect wave grouping, which could explain discrepancies between previously observed and modeled spectral widths of propagating vorticity motions. Finally, the potential enstrophy balance shows that vorticity production due to wave groups may be as important as that due to the instability process and that not all low-frequency vortical motions observed during oblique wave incidence should be attributed to shear instabilities of the alongshore current.

Citation: Long, J. W., and H. T. Özkan-Haller (2009), Low-frequency characteristics of wave group–forced vortices, *J. Geophys. Res.*, 114, C08004, doi:10.1029/2008JC004894.

1. Introduction

[2] Vorticity motions in the nearshore ocean contribute to mixing and dispersion, thus affecting the alongshore current distribution [Bühler and Jacobson, 2001] and the fate of nearshore pollutants [Spydell *et al.*, 2007]. Moreover, if vortices persist at the same location for a sufficiently long time, they can cause bathymetric change, potentially leading to rip channel development [Reniers *et al.*, 2004]. A primary generation mechanism for vortices in the surf zone was proposed by Peregrine [1998] and involves short-crested wave breaking with vortices developing where alongshore gradients in wave height exist. A long-crested incoming wavefield can develop such alongshore wave breaking variability if the surf zone bathymetry is alongshore variable, e.g., when a shore-parallel bar with incised channels is present. Such a situation has been analyzed by numerous researchers for normal or near-normal wave incidence in the laboratory [e.g., Haller *et al.*, 2002], under field conditions [e.g., MacMahan *et al.*, 2005], and theo-

retically [e.g., Brocchini *et al.*, 2004; Kennedy *et al.*, 2006; Terrile *et al.*, 2006].

[3] Alternately, similar alongshore wave breaking variability can also result (even over alongshore uniform bathymetry) if the incident wave spectrum includes a range of wave frequencies and directions. In this case, the interactions between individual wave components creates an incident wavefield with spatially and temporally varying wave heights indicative of wave groups. Under conditions involving normally incident (in the mean) but directionally spread waves, recent field observations indicate the presence of energetic eddy fields with spatial scales of 5–50 m [Spydell *et al.*, 2007], and some vortex pairs can manifest themselves as transient rip currents [Johnson and Pattiaratchi, 2004]. These observations, as well as recent model simulations [e.g., Reniers *et al.*, 2007; Spydell and Feddersen, 2009; Johnson and Pattiaratchi, 2006; Reniers *et al.*, 2004], also suggest that the resulting vorticity motions evolve slowly at time scales greater than 200 s, providing energy that populates the low-frequency range ($f < 0.005$ Hz) of the velocity spectrum. Further, numerical simulations for alongshore uniform bathymetry suggest that some vortices may even persist for durations of up to 25 min [Reniers *et al.*, 2004; Johnson and Pattiaratchi, 2006], even though the wave group time scales are much shorter. Such a long lifespan allows these vortices to potentially trigger incipient

¹College of Oceanic and Atmospheric Sciences, Oregon State University, Corvallis, Oregon, USA.

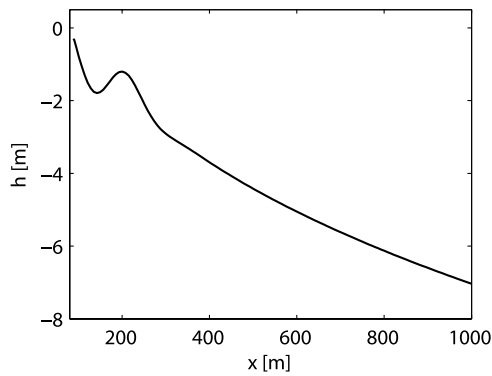


Figure 1. Alongshore uniform barred beach profile used as model bottom boundary condition.

sediment motion leading to the formation of bathymetric features such as rip channels [Reniers *et al.*, 2004].

[4] Although models predict that the vortices are persistent, a simple physical explanation for such behavior has yet to be identified. Reniers *et al.* [2004] analyze simulations for normally incident wave groups and propose that vortices generated by large wave groups are unaffected by subsequent less energetic wave groups. In that case, temporal variations in the velocity signal over many wave group periods would be characterized by a slow, steady frictional decay [Ryrie, 1983], rather than exhibit fluctuations on the scale of individual wave groups. However, this hypothesis was not tested as part of the Reniers *et al.* [2004] study and is not entirely intuitive. Herein, we propose an alternate explanation. We hypothesize that generated vortices respond to every incoming wave group and that their long-term behavior is strictly controlled by the exact sequencing of the wave groups. We utilize the potential vorticity balance to isolate the dynamics of the vorticity motions and show the correspondence between the wave group forcing and the response of individual vortices. We then expand our analysis by addressing the repercussions of these findings for cases that involve obliquely incident wave groups.

[5] Under oblique wave incidence an alongshore current is forced and energy present in the low-frequency ($f < 0.005$ Hz) range of the frequency spectrum is usually attributed to instabilities of the alongshore current. While model-data comparisons have shown that shear instability theory provides the correct alongshore propagation speed and magnitude of the observed energy, some consistent discrepancies between the theory and observations exist [see Noyes *et al.*, 2005; Özkan-Haller and Kirby, 1999]. For example, the modeled low-frequency motions occupy a narrow ridge in the frequency-wave number spectrum, whereas the observed spectrum is much broader. Also, some previous observations of vorticity motions in the surf zone cannot be explained by shear instability theory because the measured current shear on the seaward side of the alongshore current peak is too weak and the alongshore current is therefore stable [Dodd *et al.*, 1992]. A few alternate mechanisms for the generation of low-frequency vorticity motions for oblique waves have been suggested. For example, Fowler and Dalrymple [1990] considered group waves that are a result of two intersecting wave

trains at slightly different frequencies and directions. They found that a slowly migrating circulation system with a low-frequency signature can result. Haller *et al.* [1999] considered the effect of wave group forcing on the linear instability of the alongshore current and suggested that vortical motions generated by wave groups may either provide the necessary initial perturbation for instabilities, or act as a source of low-frequency vorticity energy when the alongshore current is otherwise stable. Both of these studies explore an aspect of wave group forcing in oblique wave cases, but the theoretical treatment in both studies is highly simplified. Further, nonlinear model simulations analyzing forced vortex dynamics for obliquely incident directionally spread waves have, to date, not been discussed in the literature. Here, we will analyze such simulations under conditions involving both stable and unstable wave-induced alongshore currents. The analysis also shows that when multiple coexisting mechanisms for vorticity generation in the surf zone exist, the potential enstrophy balance proves valuable in separating their individual contributions.

[6] In summary, in this study we concentrate on cases involving directionally spread waves incident on an alongshore uniform beach and theoretically address three questions.

[7] 1. What controls the lifespan of vortices? Are the temporal variations of the vortices controlled by wave forcing or bottom friction?

[8] 2. What is the effect of wave group-forced vortices on the low-frequency range of the spectrum in the case of obliquely incident wave groups?

[9] 3. What is the relative importance of vorticity generation due to shear production versus wave group forcing in cases of obliquely incident wave groups?

[10] We begin with a brief description of the numerical models (section 2) and analysis techniques (section 3) used in this study. Vortex dynamics are examined using simplified cases in section 4 to provide a baseline understanding of vortex behavior under controlled conditions. We then present simulations using both normally and obliquely incident random wavefields in section 5. A summary of our conclusions and implications of this research are then provided in section 6.

2. Model Description

[11] We utilize the conservation of wave energy principle to model the evolution of incident wave groups and employ a wave-induced circulation model based on the phase-averaged, depth-integrated Navier Stokes equations. Our approach is similar to the modeling scheme employed by Reniers *et al.* [2004] and follows the work of Özkan-Haller and Li [2003]. The governing equations are discussed only briefly, and emphasis is given to aspects that differ from those of Özkan-Haller and Li [2003].

[12] The model domain is characterized by an alongshore uniform barred bathymetry as given by Reniers *et al.* [2004] (Figure 1). The bathymetry is composed of a submerged bar superimposed on a power law beach profile. The bar crest is located 110 m offshore ($x = 200$ m) with a local water depth over the bar crest of 1.2 m. The model grid and boundary conditions vary slightly between simulations and are individually defined in sections 4 and 5. The model uses a time

step of 0.05 s, and modeled quantities are saved at 10 or 20 s intervals, depending on the total length of the simulation.

2.1. Wave Model

[13] The evolution of the incoming wave group energy is modeled using a phase-averaged wave model based on the conservation of wave energy principle.

$$\frac{\partial E}{\partial t} + \frac{\partial(Ec_g \cos \theta)}{\partial x'} + \frac{\partial(Ec_g \sin \theta)}{\partial y'} = -\epsilon_b \quad (1)$$

The reference frame is such that x' is positive shoreward and y' follows a right-handed coordinate system. Wave energy is denoted by E and is allowed to vary spatially and temporally because of the presence of wave groups. The incident wave angle, θ , is measured counterclockwise from the x' axis and is computed over the entire domain using the irrotationality of wave number principle, thus accounting for depth-induced refraction. The wave group velocity (c_g) is computed using the linear dispersion relation accounting for the total water depth, $d = h + \eta$, where h is the still water depth and η is the surface elevation associated with the wave-induced circulation.

[14] Several formulations are available to parameterize the dissipation due to depth-limited wave breaking (ϵ_b). One such formulation involves the consideration of a saturated surf zone and would, therefore, involve a moving break-point with sharp spatial gradients in breaking dissipation and no wave grouping inside the surf zone. However, observations show that waves in fact display groupiness in the surf zone [e.g., *List*, 1991], indicating that the use of saturated wave breaking is not appropriate. Alternately, wave breaking dissipation can be parameterized using a bulk wave dissipation formulation for a random wavefield [e.g., *Thornton and Guza*, 1983; *Battjes and Janssen*, 1978]. Such a formulation produces spatially smooth breaking dissipation and is hence not strictly applicable to the situation of wave groups, but generally reproduces the reduction (but not complete extinction) of wave grouping in the surf zone. The dissipation formulation of *Roelvink* [1993] also produces a smooth dissipation function and has been applied by *Reniers et al.* [2004], whose work, in part, motivated this paper. Herein, we incorporate the wave breaking dissipation formulation of *Thornton and Guza* [1983] and produce results that closely correspond to the simulations of *Reniers et al.* [2004].

[15] In contrast to *Özkan-Haller and Li* [2003] but in accordance with *Reniers et al.* [2004], we neglect all other effects of the circulation on the incident wavefield. Hence, in its present form, the model accounts for the effects of wave shoaling and refraction due to bathymetric variations and depth-limited wave breaking but neglects wave diffraction and wave height variations due to wave-current interaction. We have performed some basic tests to evaluate the effect of wave-current interaction on the low-frequency characteristics of the wave group-forced vortices. While some of the flow velocities were modified when wave-current interaction is considered, the results presented here regarding the temporal characteristics of these vortical motions were unchanged.

2.2. Circulation Model

[16] The circulation model solves the time-averaged non-linear shallow water equations which include the effects of unsteady incident wave forcing (radiation stress gradients), bottom friction, and lateral momentum mixing.

$$\frac{\partial \eta}{\partial t} + \frac{\partial}{\partial x} [u(h + \eta)] + \frac{\partial}{\partial y} [v(h + \eta)] = 0 \quad (2)$$

$$\frac{\partial u}{\partial t} + u \frac{\partial u}{\partial x} + v \frac{\partial u}{\partial y} = -g \frac{\partial \eta}{\partial x} + \tau_{w_x} + \tau_{m_x} - \tau_{b_x} \quad (3)$$

$$\frac{\partial v}{\partial t} + u \frac{\partial v}{\partial x} + v \frac{\partial v}{\partial y} = -g \frac{\partial \eta}{\partial y} + \tau_{w_y} + \tau_{m_y} - \tau_{b_y} \quad (4)$$

In the above set of equations, u and v are the cross-shore and alongshore components of velocity in the $x - y$ right-handed coordinate axes. Positive values of x point offshore in this reference system. Model velocities are a combination of the wave induced drift velocity \vec{u}_S and the Eulerian particle velocity \vec{u}_E ,

$$\vec{u} = \vec{u}_S + \vec{u}_E, \text{ where } \vec{u}_S = \frac{\vec{Q}_w}{(h + \eta)} \quad (5)$$

and \vec{Q}_w is defined as the shoreward directed mass flux due to the waves. The wave forcing, τ_{w_x} is computed using radiation stress gradients as expressed by *Longuet-Higgins and Stewart* [1964]:

$$\begin{aligned} \tau_{w_x} &= -\frac{1}{\rho d} \left(\frac{\partial S_{xx}}{\partial x} + \frac{\partial S_{xy}}{\partial y} \right) \\ \tau_{w_y} &= -\frac{1}{\rho d} \left(\frac{\partial S_{xy}}{\partial x} + \frac{\partial S_{yy}}{\partial y} \right) \end{aligned} \quad (6)$$

where S_{xx} , S_{xy} and S_{yy} denote the components of the radiation stress tensor and are computed using linear water wave theory. Lateral momentum mixing (τ_m) is parameterized using an eddy viscosity term with $\nu_t = Md (\epsilon_b/\rho)^{1/3}$. In this parametrization, ϵ_b represents the breaking wave dissipation, ρ is the water density, and M is the lateral mixing coefficient [*Battjes*, 1975]. One modification to the model over previous versions [e.g., *Özkan-Haller and Li*, 2003] is the inclusion of a nonlinear representation for the bottom friction that does not rely on either a weak- or strong-current assumption. Following the work of *Feddersen et al.* [2000], the nonlinear bottom friction dissipation is parameterized using

$$\vec{\tau}_b = \frac{c_f}{d} \langle \vec{u}|\vec{u} \rangle = \frac{c_f}{d} \sigma_T \vec{u} \left[1.16^2 + (\vec{u}/\sigma_T)^2 \right]^{1/2}. \quad (7)$$

The depth-dependent spatially variable friction coefficient c_f is expressed by the Manning-Strickler equation $c_f = 0.015 \left(\frac{k_a}{d} \right)^{1/3}$ [*Sleath*, 1984]. In this formulation, $\langle \rangle$ represents the time average and we use linear wave theory to compute the wave-orbital velocity variance, σ_T . We use a roughness value of $k_a = 0.022$ which corresponds to $c_f = 4.0 \times 10^{-3}$

over the crest of the bar. This is consistent with measured values of c_f [e.g., *Garcez Faria et al.*, 1998], although we acknowledge that there are uncertainties and considerable variability in the appropriate friction coefficient. We have tested the sensitivity of our conclusions to the size of the bottom friction coefficient, increasing and decreasing it by a factor of two and found that in all cases where waves are continually present, the bottom friction component, while important, does not dictate the temporal variability of vortical motions.

[17] *Feddersen et al.* [2000] tested the form given in equation (7) for only the alongshore component of the bottom shear stress. However, the original expression by *Wright and Thompson* [1983] was formulated for a bottom shear stress vector that was aligned with the direction of the flow, and it is in this spirit that the parameterization is used here. We note that we also incorporated several different bottom stress parameterizations including a linear weak-current parameterization and a nonlinear strong-current parameterization in addition to the hybrid parameterization of *Feddersen et al.* [2000]. In all cases, our conclusions regarding longevity and temporal characteristics of the wave group–forced surf zone vortices remain unchanged.

3. Analysis Methods

[18] We utilize several analysis methods to assess the different characteristics of the surf zone vortices. In particular, we use the potential vorticity balance as a diagnostic tool to assess the nature of the forcing and dissipation of wave group–forced vortices. The potential vorticity balance has been used successfully by previous studies to highlight similar dynamic relationships. For example, *Johnson and Pattiaratchi* [2006] used this balance to show that the main forcing of vorticity due to wave grouping occurs inside the surf zone. Also, *Bühler and Jacobson* [2001] used the potential vorticity balance to describe the life cycle of an isolated vortex from its generation to its eventual demise. Herein, we integrate the potential vorticity balance over the area of a vortex in order to isolate the relative importance of wave forcing and bottom friction in dictating the temporal evolution of the isolated vortex. This analysis is helpful in examining a previous hypothesis by *Reniers et al.* [2004] that suggests that bottom friction should be responsible for the temporal evolution of a given vortex.

[19] An area-averaged or vortex-tracking balance by default minimizes the role of advective changes in potential vorticity because the area of interest always contains the moving vortex. To determine the relative importance of local and advective changes in potential vorticity, we analyze the balance of potential vorticity at isolated spatial locations. In the vicinity of the bar, such balances indicate when a “forced” balance exists (where the total time rate of change of vorticity is balanced largely by wave forcing) or when the vortices are “free” (characterized by nearly conserved potential vorticity and, therefore, a balance between the local and advective acceleration of potential vorticity). Further, consideration of point balances at a particular cross-shore location (as a function of alongshore location and time) also enables us to look at the dynamics of individual vortices over the bar and assess reasons for their longevity.

[20] In addition to the potential vorticity balance, we also evaluate the potential enstrophy balance (potential vorticity squared) to identify the dominant sources (positive definite quantities) and sinks (negative definite quantities) of vortical motions over the whole domain [e.g., *Terrile et al.*, 2006; *Zhao et al.*, 2003]. The potential enstrophy balance also separates the contribution of vortices generated by multiple mechanisms. The relationship between vorticity and enstrophy is analogous to the relationship between velocity and kinetic energy. Some previous studies have used a kinetic energy balance that employs a rigid lid assumption to evaluate the dynamics of nearshore vortical motions [e.g., *Dodd and Thornton*, 1990; *Allen et al.*, 1996]. In our case, the incident wave groups force gravity motions in addition to the vortices of interest. The kinetic energy balance includes a substantial contribution from these gravity motions (for which a rigid lid assumption is not appropriate), and, therefore, does not clearly elucidate the dynamics of the vorticity motions. Separating the dynamics of the gravity and vorticity motions in the kinetic energy balance is possible but not trivial. Instead, the enstrophy balance elegantly isolates the dynamics of the vorticity motions and enables an analysis of the contribution of shear production and direct forcing to the generation of the simulated vorticity field.

3.1. Potential Vorticity Balance

[21] The vorticity balance is derived by cross differentiating and subtracting the depth-averaged momentum equations (equations (3) and (4)). We divide the resulting equation by the total water depth ($d = h + \eta$), and invoke the continuity equation to simplify the expression. After rearranging, we arrive at an equation for the conservation of potential vorticity.

$$-\frac{D\zeta}{Dt} + \frac{1}{d} \nabla_h \times [\overline{\tau_w} + \overline{\tau_m} - \overline{\tau_b}] = 0 \quad (8)$$

In this equation, the potential vorticity is given by $\zeta = \frac{q}{d}$, where q is the vorticity defined as $q = \frac{\partial v}{\partial x} - \frac{\partial u}{\partial y}$ and ∇_h represents the horizontal gradient operator. $\frac{D()}{Dt}$ denotes the total derivative which we will refer to as the total time rate of change of potential vorticity and the components of the material derivative, $\frac{\partial \zeta}{\partial t}$ and $u \frac{\partial \zeta}{\partial x} + v \frac{\partial \zeta}{\partial y}$, correspond to the local and advective changes of potential vorticity, respectively.

3.2. Potential Enstrophy Balance

[22] We follow the derivation of *Zhao et al.* [2003] but begin with the conservation of potential vorticity rather than the conservation of vorticity considered by them. We first separate the potential vorticity balance into alongshore mean and fluctuating components denoted by an overbar and prime, respectively:

$$\begin{aligned} \zeta &= \bar{\zeta} + \zeta'; & u &= \bar{u} + u'; & v &= \bar{v} + v'; \\ \frac{1}{d} \nabla_h \times \tau_\beta &= \left(\frac{1}{d} \nabla_h \times \tau_\beta \right) + \left(\frac{1}{d} \nabla_h \times \tau_\beta \right)', \end{aligned} \quad (9)$$

where β is used to represent the wave forcing, turbulent mixing, and bottom stress. We alongshore average this full potential vorticity equation to define the local mean potential vorticity balance. The assumption of periodicity in the alongshore direction simplifies the derivation by eliminating y derivatives of alongshore averaged quantities. The potential enstrophy perturbation equation is then derived by subtracting the alongshore averaged potential vorticity equation from the full potential vorticity equation and multiplying by the perturbation potential vorticity and alongshore averaged total water depth ($\zeta\bar{d}$). The resulting equation is alongshore averaged and cross-shore integrated from the bar trough (x_t) to the offshore boundary (L_x) and simplified by invoking the mean and perturbation continuity equations. While *Zhao et al.* [2003] integrate over the entire cross-shore domain, we exclude the area near the shoreline in the integration because a separate set of vortices are forced there because of renewed wave breaking, and our simplified shoreline treatment inhibits realistic treatment in that region. Vortices generated on the bar and near the shoreline are clearly separated by the presence of the bar trough where the vorticity is minimal and can therefore be neglected. Hence, by assuming zero vorticity in the bar trough and at the offshore boundary, the cross-shore integral of the two x derivative terms in the equation that describe the advection of enstrophy will be identically zero, as they were for *Zhao et al.* [2003]. We have verified, by computing the advection terms in the enstrophy balance, that our assumption of zero vorticity in the bar trough is valid and that they do not contribute to the balance of enstrophy. The perturbation enstrophy balance (equation (10)) derived in this manner describes the balance of enstrophy associated with vortical motions generated by the wave group forcing and shear instabilities, if present.

$$\begin{aligned} \int_{x_t}^{L_x} -\frac{\partial}{\partial t} \left(\frac{1}{2} \zeta' \zeta' \bar{d} \right) dx - \int_{x_t}^{L_x} \overline{\zeta' u' \bar{d} \frac{\partial \zeta}{\partial x}} dx \\ + \int_{x_t}^{L_x} \bar{d} \zeta' \overline{\left(\frac{1}{d} \nabla_h \times \vec{\tau}_w \right)'} dx \\ + \int_{x_t}^{L_x} \bar{d} \zeta' \overline{\left(\frac{1}{d} \nabla_h \times \vec{\tau}_m \right)'} dx \\ - \int_{x_t}^{L_x} \bar{d} \zeta' \overline{\left(\frac{1}{d} \nabla_h \times \vec{\tau}_b \right)'} dx = 0 \end{aligned} \quad (10)$$

[23] Here, the first term represents changes in the local rate of change of perturbation potential enstrophy (ENS_t). The second and third terms define the production of potential enstrophy by the shear in the mean alongshore current ($PROD_{shear}$) and the perturbation wave forcing (i.e., wave groups) ($PROD_{wave}$), respectively. The fourth term accounts for turbulent mixing of the perturbation potential enstrophy (MIX) and the last term represents the contribution due to the curl of the bottom stress ($FRIC$). This is similar to equation (B10) given by *Zhao et al.* [2003] except it was derived in terms of potential vorticity; hence vortex stretching terms are absent. Analysis of this balance will identify those components that act as sources or sinks of potential enstrophy as well as establish the ratio of potential enstrophy production from both the wave group forcing and

the shear production due to the mean alongshore current. Hereinafter, reference to the potential enstrophy balance will pertain to the perturbation potential enstrophy equation given in equation (10).

3.3. Vortex Tracking

[24] In the simplified cases that follow, the wave groups have a fixed alongshore structure. Therefore the vortex generation location is dictated by the alongshore nodal positions of the wave groups. In these cases a control area that encompasses one half of a rip current cell and extends from the bar crest to the offshore boundary is used. Our goal is to evaluate, in a controlled situation, the relative importance of wave forcing and bottom friction in dictating the temporal variations of the wave group-forced vortices. The simplicity of using an area integral must be abandoned when stochastic nearshore flows are considered, and instead we adopt the vortex tracking algorithm developed by *McWilliams* [1990] for use in the study of coherent vortices in 2-D turbulence. With this we can follow each vortex through space and time and evaluate the integrated potential vorticity balance for any given vortex. This analysis helps us evaluate the forces that affect any chosen vortex as it is generated, propagates and degenerates.

[25] For each model output time, the algorithm first identifies all extrema (ζ_e) in the domain that exceed a chosen threshold value. The algorithm then searches for all the boundary points surrounding each extremum. The boundary is defined as

$$\zeta/\zeta_e = \Delta \quad (11)$$

where $\Delta = 0.25$ for this study. Vortices with boundaries that are not identified as closed curves are rejected.

[26] After identifying the boundary of each vortex, overlapping or redundant vortices are combined or eliminated. We also neglect any vortices positioned at the lateral boundaries and restrict the analysis to vortices seaward of the bar trough. The acceptable values used for shape parameters in this study are much less stringent than those used by *McWilliams* [1990] because that study was concerned with axisymmetric circular vortices, whereas we allow vortices of practically any shape to be included in the analysis. For this study we use only two of the shape tests, the first of which requires that the vortex area (A) exceed 750 m^2 . The second test evaluates the circularity (R) of the vortex boundary where $R = C/(2\sqrt{\pi A})$ and C is the circumference of the vortex. A value of $R = 1$ corresponds to a perfect circle and increasing values of R indicate more complex boundary shapes. For this study we use a value of $R = 2.5$ as our upper bound. Changing the parameters we use in the vortex tracking algorithm will only change the number of vortices identified or slightly alter the size of the vortices (dictated by equation (11)). Because neither of these (number or size) are related to the results of the study, these subjective components of the method are inconsequential.

[27] We tested both control area methods using one of the simplified cases, and the potential vorticity balances differed by less than 0.5%. Therefore, the vortex tracking

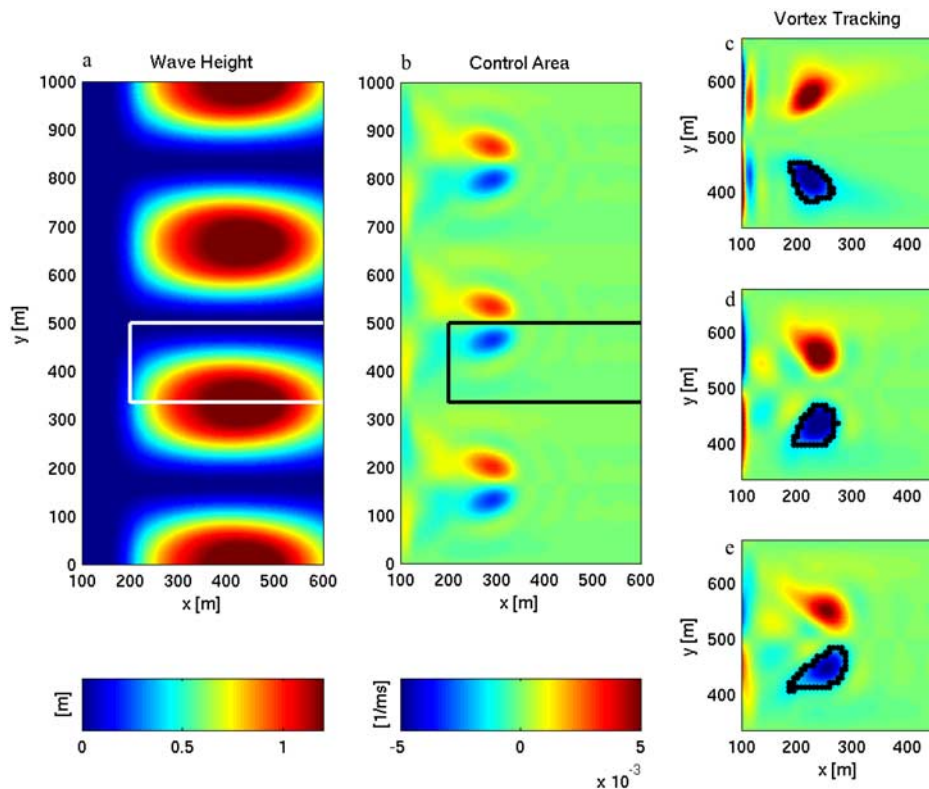


Figure 2. Single wave group. (a) Incoming wave height distribution at $t = 7.5$ min. (b) Potential vorticity $[\frac{1}{ms}]$ over the entire domain at $t = 25$ min. White and black lines denote the control area used in computing the potential vorticity balance for idealized simulations. Snapshots of the potential vorticity field at (c) $t = 8.17$ min, (d) $t = 14$ min, and (e) $t = 19.83$ min. In Figures 2c–2e, the black line outlines the same vortex identified with the tracking analysis.

method will be employed for the analysis of a stochastic field of nearshore vortices in section 4.

4. Idealized Wave Groups

4.1. Single Wave Group

[28] We begin by looking at a case with an alongshore variable, single wave group impulse, similar to the work of *Ryrie* [1983] who showed that an isolated oblique wave group would excite two primary motions: (1) edge waves propagating alongshore and (2) a steady vortex pair located at the wave group breaking location that would decay on a frictional time scale. Consequently, when considering more realistic conditions, if an existing strong vortex is unaltered by subsequent weaker wave groups, a similar frictional decay would control the temporal evolution of the vortex and manifest itself as a low-frequency signal in a spectral analysis. To illustrate this effect, we use shore-normal incident waves with a period of 10 s with 12 waves in a single wave group.

[29] The spatial grid is 1000 m \times 1000 m (cross-shore \times alongshore) with variable cross-shore spacing of 1.25–7.3 m (grid points are more concentrated at the onshore/offshore boundaries) and an alongshore spacing of 7.81 m. Walls are specified at the lateral boundaries and an open offshore boundary condition is employed. A wall boundary is also used at the shoreline, hence swash zone excursions are not included. For the case involving a single wave group, an

alongshore length scale is imposed by the incident wave-field such that three rip currents are generated at alongshore positions that correspond to the nodal locations of the incoming group. The control area used to analyze the vorticity balance is shown in Figures 2a and 2b. Because of symmetry, the results apply to the other vortices in the system as well.

[30] The potential vorticity balance for the isolated vortex (Figure 3) shows that, in this simplified case, the arrival of the wave group drives the total time rate of change of potential vorticity. Once wave forcing ceases, this total time rate of change is balanced by frictional effects. The potential vorticity balance is computed as an integral quantity, but the potential vorticity extremum in the control area (ζ_e) is also given for reference. The resulting potential vorticity time series indicates that the vortex decays slowly under the influence of bottom friction with an e-folding time scale of 14.33 min. The decay rate is directly related to the size of the bottom friction term, and hence the bottom roughness. A fivefold increase in the bottom roughness results in a decrease in the e-folding time scale to 2.67 min. We note that for this case the term associated with lateral momentum mixing does not contribute significantly.

[31] The chosen control area allows us to isolate the relative importance of wave forcing and bottom friction in dictating the total rate of change of potential vorticity, but it does not allow us to assess the relative role of the local and advective potential vorticity changes. For this purpose, we

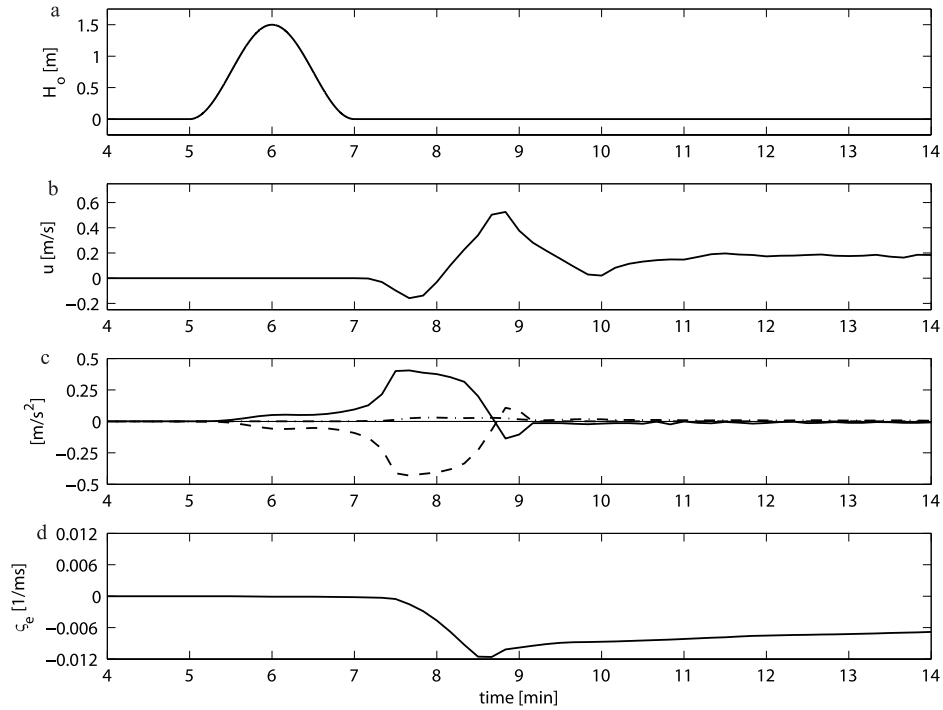


Figure 3. Single wave group. (a) Time series of the offshore wave group height at $y = 335$ m. (b) Cross-shore velocity time series observed at $x = 222$ m, $y = 500$ m. (c) The potential vorticity balance for a control area between $335 < y < 500$ m. Solid line, $-\frac{D\zeta}{Dt}$; dashed line, $\frac{1}{d}\nabla_h \times \vec{\tau}_w$; dash-dotted line, $-\frac{1}{d}\nabla_h \times \vec{\tau}_b$. (d) The potential vorticity extremum in the control area (ζ_e).

also analyze the balance computed at a single point just offshore of the bar crest (Figure 4). As the wave group approaches the bar and begins to break, the curl of the wave forcing is balanced by the local change (i.e., strengthening) of potential vorticity. This balance is indicative of a forced motion. Advective changes are small at first because the vortex is relatively stationary, but they become important once the vortex begins to move because of mutual advection with its neighboring vortex. As the tail of the wave group propagates through, the associated negative cross-shore gradients cause a reversal in the sign of the curl of the radiation stress gradients. This effect results in the active weakening of the generated vortex. After the passage of the wave group, the total rate of change of potential vorticity is

balanced by frictional effects, although both of these terms are small and potential vorticity is nearly conserved. Therefore, as the vortex continues to move offshore, the local and advective potential vorticity changes are nearly in balance which is indicative of a free motion. We note that the size of the local and advective terms at this location are representative of their size at any point in the domain.

4.2. Wave Group Sequences

[32] An initial objective of this research is to illustrate how wave groups arriving at later times will affect vortices that were generated by preceding wave groups. Hence, we conducted a series of idealized simulations aimed to analyze the vortex characteristics resulting from sequences of wave

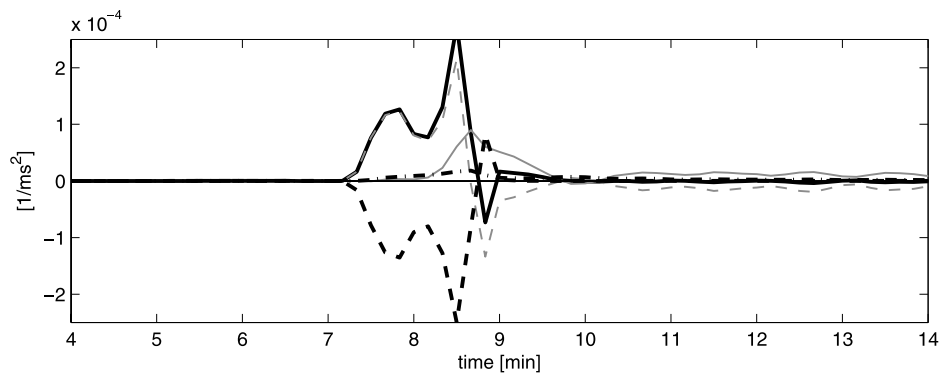


Figure 4. Single wave group. Potential vorticity balance computed at a single point ($x = 223$ m, $y = 406$ m). Black solid line, $-\frac{D\zeta}{Dt}$; gray dashed line, $-\frac{\partial\zeta}{\partial t}$; gray solid line, $-(u\frac{\partial\zeta}{\partial x} + v\frac{\partial\zeta}{\partial y})$; black dashed line, $\frac{1}{d}\nabla_h \times \vec{\tau}_w$; black dash-dotted line, $-\frac{1}{d}\nabla_h \times \vec{\tau}_b$.

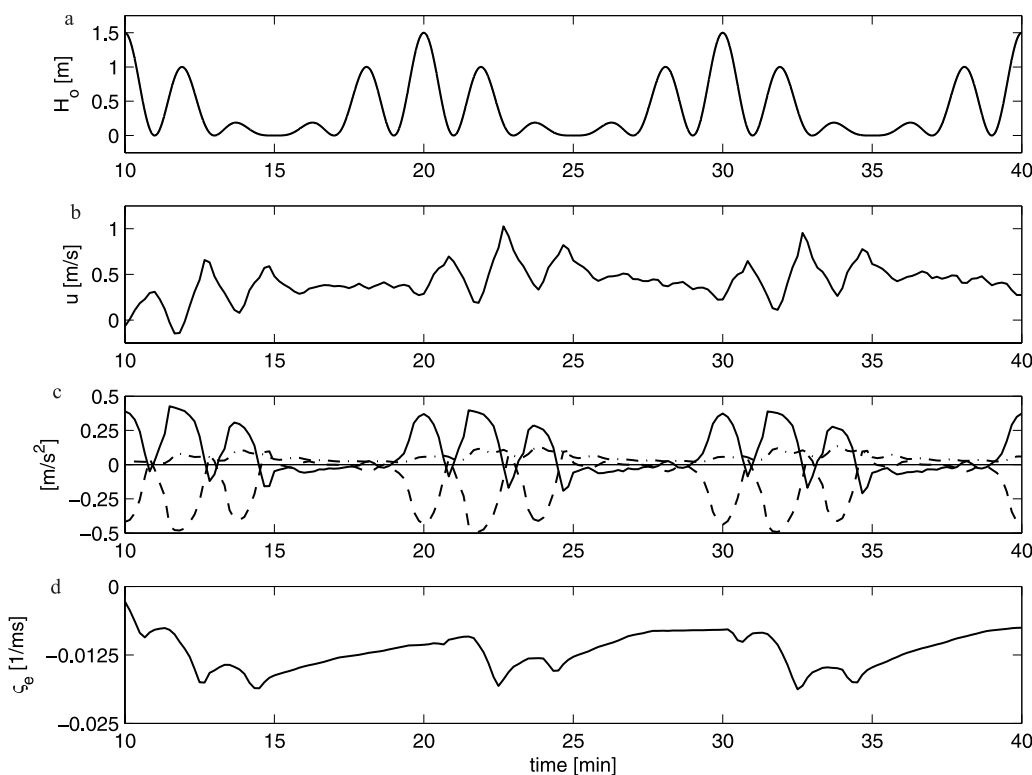


Figure 5. Simplified wave group sequence. (a) Time series of the offshore wave group height at $y = 335$ m. (b) Cross-shore velocity time series observed at $x = 222$ m, $y = 500$ m. (c) The potential vorticity balance for a control area between $335 < y < 500$ m. Solid line, $-\frac{D_t}{Dt}$; dashed line, $\frac{1}{d}\nabla_h \times \vec{\tau}_w$; dash-dotted line, $-\frac{1}{d}\nabla_h \times \vec{\tau}_b$. (d) The potential vorticity extremum in the control area (ζ_e).

groups with varying magnitude. Mainly, is a vortex that was driven by an energetic wave group unaffected by subsequent smaller incoming wave groups, as previously suggested, or does it respond to all additional forcing? The grid and computational time step are the same as those used in the previous case. We conducted a number of numerical experiments involving individual wave groups with a period of 2 min and a long-term modulation function that defines the “shape” of the sequence (e.g., sawtooth, exponentially decaying sawtooth, sine-squared function, etc.) which repeats every 10 min. For brevity, we show the results from only one case but we note that the results were consistent among all simulations.

[33] The incoming wave groups are modulated using a sine-squared function and the alongshore structure of the wave groups is the same as that shown in the single wave group case. Figure 5 shows the time series of the offshore wave group height along with the integrated potential vorticity balance over the same area as in section 4.1. The temporal variability of the total time rate of change of potential vorticity is directly linked to the curl of the wave forcing while the curl of bottom friction has a more constant influence. The vortices respond to each subsequent breaking wave group, regardless of size, meaning there is not sufficient time for significant frictional decay to take place. Of course, given that waves must break for radiation stress forcing to be present, if a wave group is so small that it does not break over the bar, the vortex is unaffected. This is evident by the two smallest wave groups (e.g., $t = 14$ and

16 min in Figure 5) that are separating larger groups of waves. During this time, the dominant balance is between the curl of bottom friction and the total time rate of change of potential vorticity. A long separation between breaking wave groups ($O(5$ min)) would be required for a frictional decay to become significant, and whether or not such a long absence of energetic waves exists in a realistic wave spectrum will be addressed in section 5. We note here that the vorticity balance at a point (not shown) leads to conclusions similar to those described in the previous case. Namely, the advective changes in potential vorticity are small at first, but gain importance as the vortices begin to move under the influence of mutual advection and self-advection due to the sloping bathymetry. During the short periods of low wave group forcing, local and advective changes are nearly balanced. The remainder, which is the total time rate of change of vorticity, is balanced by the frictional effects.

[34] At this point we introduce the perturbation potential enstrophy balance to gain familiarity under simplified conditions. Unlike the potential vorticity balance that was integrated over a predefined control area, the potential enstrophy balance is integrated over the entire alongshore domain and from the bar trough to the offshore boundary. In this case, the mean potential enstrophy balance is trivial, and the perturbation balance essentially describes the full enstrophy budget. The potential enstrophy balance is shown in Figure 6 and elucidates the sources and sinks of enstrophy (and therefore vorticity) in the domain. We see that

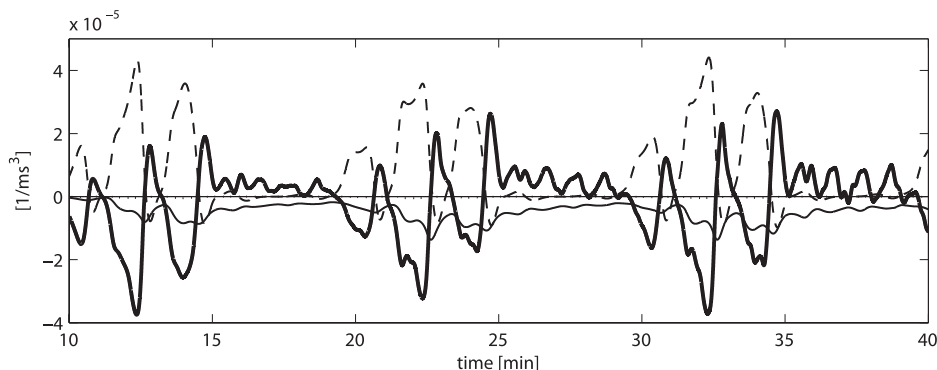


Figure 6. Simplified wave group sequence. Enstrophy balance integrated over all alongshore positions and from the bar trough to the offshore boundary. Thick solid line, ENS ; dashed line, $PROD_{wave}$; dotted line, MIX ; thin solid line, $FRIC$.

bottom friction is a negative definite quantity always acting to dissipate the enstrophy in the domain. The perturbation wave forcing (i.e., wave groups) primarily acts as the source of vorticity motions, however, when the wave group forcing term opposes the rotation direction of an existing vortex, it actively slows it down and, therefore, appears as an enstrophy sink. As discussed during the single wave group case, this can be observed during brief times when the tail of each breaking wave group reverses the sign of the wave forcing term, thereby causing a corresponding decay in the perturbation enstrophy. Similar to the analysis of the potential vorticity equation, there is a general correspondence between the time variations of the incident wave group forcing and the time rate of change in potential enstrophy.

[35] We note that, like those given by *Reniers et al.* [2004], the time series of offshore wave height and cross-shore velocity in the surf zone (Figure 5) show little correspondence. Our results indicate that such a lack of correspondence is not indicative of the absence of a direct dynamical relationship between the wave forcing and response as previously interpreted by *Reniers et al.* [2004]. Instead, other motions such as edge waves are present in the velocity signal in the surf zone that inevitably mask this relationship. It can, however, be demonstrated when the potential vorticity or potential enstrophy balance is considered.

5. Random Wave Groups

[36] In the previous cases, the nodes and antinodes of the successive wave groups occurred at fixed alongshore positions. Hence, the generated vortices were repeatedly strengthened by each successive wave group. In a random wavefield we expect vortices to be generated at random alongshore positions, and the effect of subsequent wave groups (with nodes and antinodes at different positions than the previous groups) would provide both constructive and destructive forces.

[37] For these cases, a random wavefield is generated from a TMA spectrum [*Bouws et al.*, 1985] with a significant wave height of 1.4 m ($H_{rms} = 1$ m) and a peak period of 10 s. We use a spectral spreading parameter (γ) of 7, resulting in a relatively narrow spectrum. The peak direction of the spectrum varies as described for each case. Following *Reniers et al.* [2004], we derive the time-dependent offshore

wave group envelope using the procedure described by *Van Dongeren et al.* [2003]. According to this representation, the incident water surface elevation (η_s) at each offshore grid point is expressed as the summation of wave components, each with a given frequency (f), amplitude (B), direction (θ), and random phase (ϕ). We utilize 420 wave components and η_s is given by

$$\eta_s(0, y', t) = \sum_{i=1}^{N=420} B_i \cos(k_i \sin(\theta_i) y' - 2\pi f_i t + \phi_i). \quad (12)$$

In this equation, the wave number, k , is computed using the linear dispersion relationship and y' corresponds to the alongshore direction in the wave model coordinate system discussed in section 2.1. Following *Van Dongeren et al.* [2003], the wave components used in generating the water surface elevation time series are restricted to those that contain at least 10% of the peak energy density. Each chosen frequency bin is subdivided into ten smaller segments resulting in a frequency resolution of 10^{-4} Hz. A directional component corresponding to each frequency within a bin is chosen using a probability density function that follows a directional spreading function given by

$$P(\theta) = \int_{-\pi/2}^{\pi/2} \cos(\theta - \theta_{peak})^{13.5} d\theta \quad (13)$$

Therefore, components closer to the peak direction are more likely to be chosen. Note that equation (13) results in a spectrum with a directional spread equivalent to test 002 of *Reniers et al.* [2004]. Finally, the amplitude associated with each component is found by integrating the spectral density within the given frequency and direction bin. To obtain the offshore wave envelope used to initialize the wave model we take a Hilbert transform of this instantaneous water surface elevation time series at each location along the offshore boundary and low pass the signal at $f = 0.02$ Hz. We measure the amount of groupiness in the wave amplitude time series according to a groupiness factor (GF) defined by *List* [1991] as $\sqrt{2\sigma_A/\bar{A}}$ where σ_A and \bar{A} are the standard deviation and mean of the time series, respectively. The generated time series have GF values of 0.6–0.63. For reference, a quick analysis of wave height

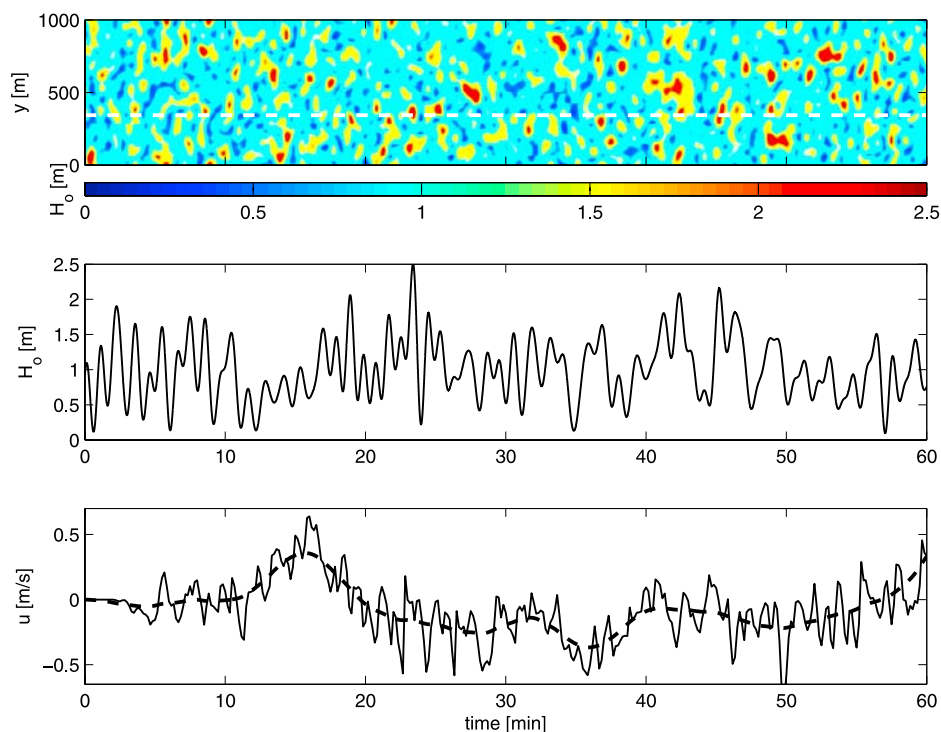


Figure 7. Normally incident random wave group sequence. (top) Time-space plot of root-mean-square wave height at the offshore boundary with $GF = 0.63$, where the white line denotes the location of (middle) the time series at $y = 344$ m. (bottom) Time series of cross-shore velocity (solid line) and low-pass-filtered ($T > 200$ s) cross-shore velocity (dashed line) at $x = 223$ m, $y = 344$ m (inside the surf zone).

time series from the Sandyduck experiment in Duck, North Carolina, indicates that a $GF = 0.7$ can be common. Here, the spatial grid is $700 \text{ m} \times 1000 \text{ m}$ (cross-shore \times alongshore) with variable cross-shore spacing of 1.25 – 4.90 m and an alongshore spacing of 7.81 m.

5.1. Normal Incidence

[38] As anticipated, the field of vortices generated by a normally incident random wavefield is much more complicated. A space-time plot (or time stack) of the offshore wave height is given in Figure 7 and indicates that wave groups will break (and consequently force either positive or negative vorticity) at variable alongshore positions. Figure 7 also shows a time series of the incident wave height at the offshore boundary along with a time series of the resulting cross-shore velocity inside the surf zone. Like *Reniers et al.* [2004], we observe a low-frequency signal in the velocity time series that is not easily identified in the offshore wave signal at the same alongshore position. We note that a comparison using the local wave height in the surf zone yields a similar disparity. Instead, the potential vorticity balance at any point on top of or seaward of the bar crest (see Figure 8, top) indicates that the total time rate of change of potential vorticity is dictated by the curl of the radiation stress forcing.

[39] The relative importance of the local and advective changes of potential vorticity can be more easily identified if we apply a lowpass filter (using a running boxcar averaging window of width 200 s) to each term in the potential vorticity balance. In this case, several types of

balances can be identified (see Figure 8, middle). At times (e.g., $t \approx 45$ min) the local time rate of change of vorticity is balanced by the wave forcing, and the advective contributions to the change in potential vorticity are small. This occurs when a vortex is strengthened by an incoming wave group but remains stationary in space. At other times (e.g., $t \approx 35$ min), a free balance between the local and advective changes of potential vorticity is evident. This occurs at times when the wave forcing term is weak, and the situation is indicative of a vortex moving across the point of interest. Any small remainder in that balance is accounted for by the bottom stress. Finally, the wave forcing term can also be primarily balanced by the advective change in the potential vorticity (e.g., $t \approx 15$ min), with only small local changes of vorticity. This indicates a situation where a vortex moves across the point of interest while changing if it encounters a breaking wave group. Overall, the time series reveal that there is a low-frequency component in the curl of the wave forcing that gives rise to the low-frequency signal observed in the total changes (local and advective) of potential vorticity, and hence in the vorticity itself.

[40] The perturbation potential enstrophy integrated over all alongshore positions from the bar trough to the offshore boundary (Figure 9) indicates that the wave forcing is the only source of potential enstrophy because shear production is zero in the absence of any mean vorticity. Both the instantaneous and the low-pass-filtered balances indicate that the temporal variations in the time rate of change of potential enstrophy are caused by the variations in the wave group forcing. Bottom friction still maintains an active role

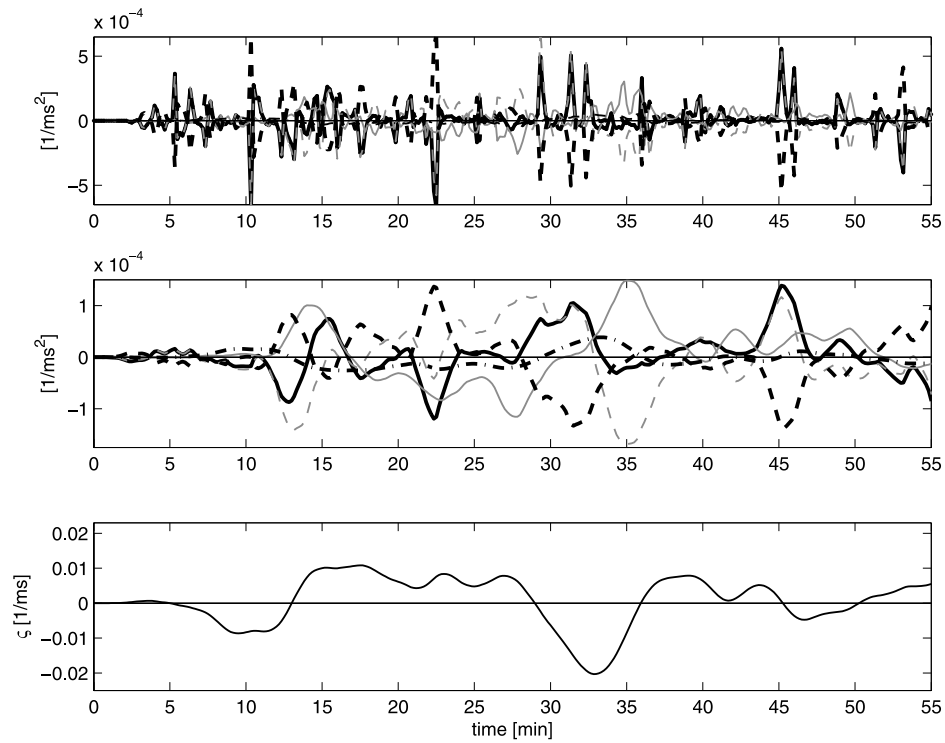


Figure 8. Normally incident random wave group sequence. (top) Potential vorticity balance computed at a single point ($x = 223$ m, $y = 344$ m). Black solid line, $-\frac{D\zeta}{Dt}$; gray dashed line, $-\frac{\partial\zeta}{\partial t}$; gray solid line, $-(u\frac{\partial\zeta}{\partial x} + v\frac{\partial\zeta}{\partial y})$; black dashed line, $\frac{1}{d}\nabla_h \times \vec{\tau}_w$; black dash-dotted line, $-\frac{1}{d}\nabla_h \times \vec{\tau}_b$. Also shown is (middle) the low-pass-filtered ($T > 200$ s) potential vorticity balance and (bottom) potential vorticity, ζ , at the same location.

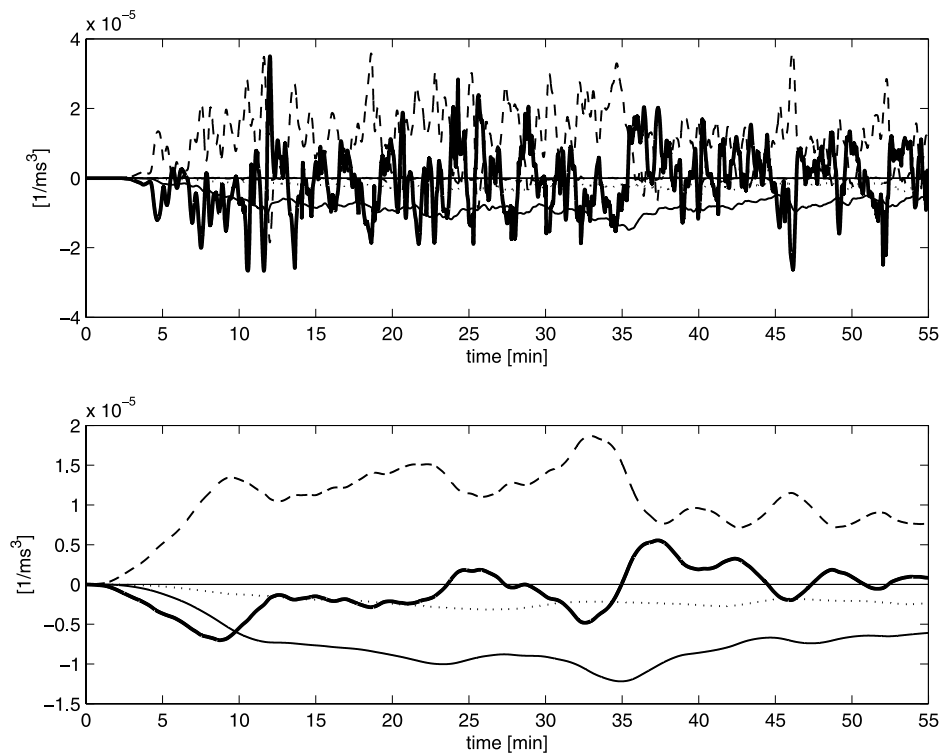


Figure 9. Normally incident random wave group sequence. (top) Entrophy balance integrated over all alongshore positions and from the bar trough to the offshore boundary. Thick solid line, ENS ; dashed line, $PROD_{wave}$; dotted line, MIX ; thin solid line, $FRIC$. (bottom) The low-pass-filtered ($T > 200$ s) potential entrophy balance.

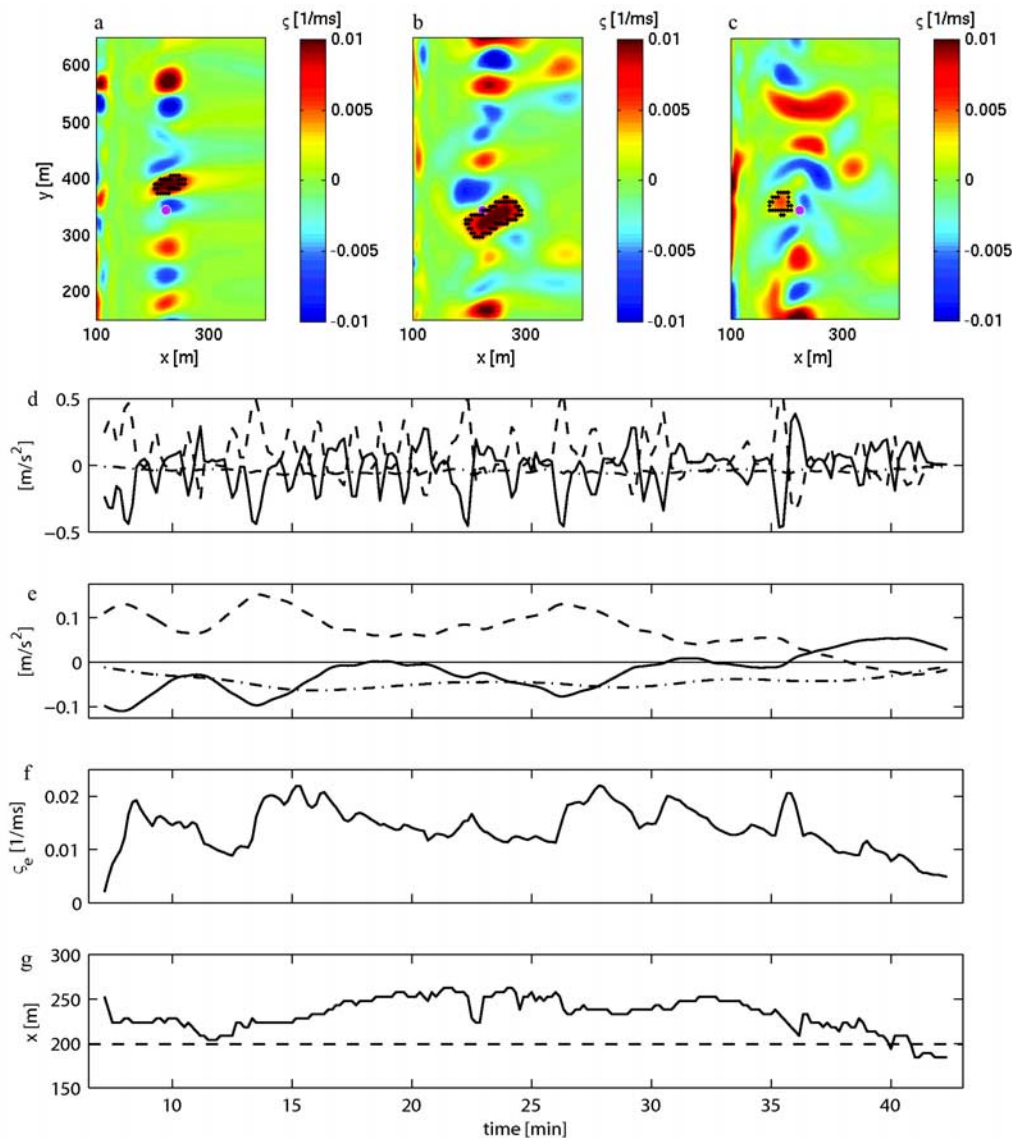


Figure 10. Normally incident random wave group sequence. Snapshots of the vortex position at (a) $t = 8.2$ min, (b) $t = 24.8$ min, and (c) $t = 41.5$ min. The magenta circle marks the location of the cross-shore velocity time series plotted in Figure 7. (d) The integrated potential vorticity balance for a vortex tracked through its lifespan. Solid line, $-\frac{D\zeta}{Dt}$; dashed line, $\frac{1}{d}\nabla_h \times \overline{\tau}_w$; dash-dotted line, $-\frac{1}{d}\nabla_h \times \overline{\tau}_b$. (e) The low-pass-filtered ($T > 200$ s) potential vorticity balance shows the long-term positive wave forcing characteristics. (f) The potential vorticity extremum (ζ_e) is given. (g) The cross-shore position of the vortex extremum (ζ_e) (solid line) relative to the bar crest (dashed line).

in the system but it varies over longer time scales and does not control the temporal variations present in the enstrophy signal.

[41] In order to address the reasons behind the longevity of any given vortex, we use the vortex tracking method (potential vorticity threshold = 0.002 m s^{-1}) to identify all the vortices and follow their initiation, evolution, and decay. The potential vorticity balance for a representative vortex (integrated over the vortex area) is shown in Figure 10. We also include three snapshots of vortex position in the model domain at arbitrary times. In this case, and all others examined in detail, a correspondence between temporal variations in the total time rate of change of potential

vorticity and the temporal variations in the curl of the wave forcing exists. This again indicates that vortices do respond to all subsequent group forcing they encounter.

[42] Although the location of the vorticity extremum migrates spatially and the vortex shape exhibits some variations, the example vortex has a lifetime of approximately 40 min, which is much longer than the time scales associated with the individual wave groups. From the potential vorticity balance we see that, as expected, when a vortex encounters wave forcing of the same sign (i.e., forcing that rotates the water column in the same direction as the existing vortex) the vortex is strengthened. Alternately, when a vortex experiences forcing of opposite sign (rotating

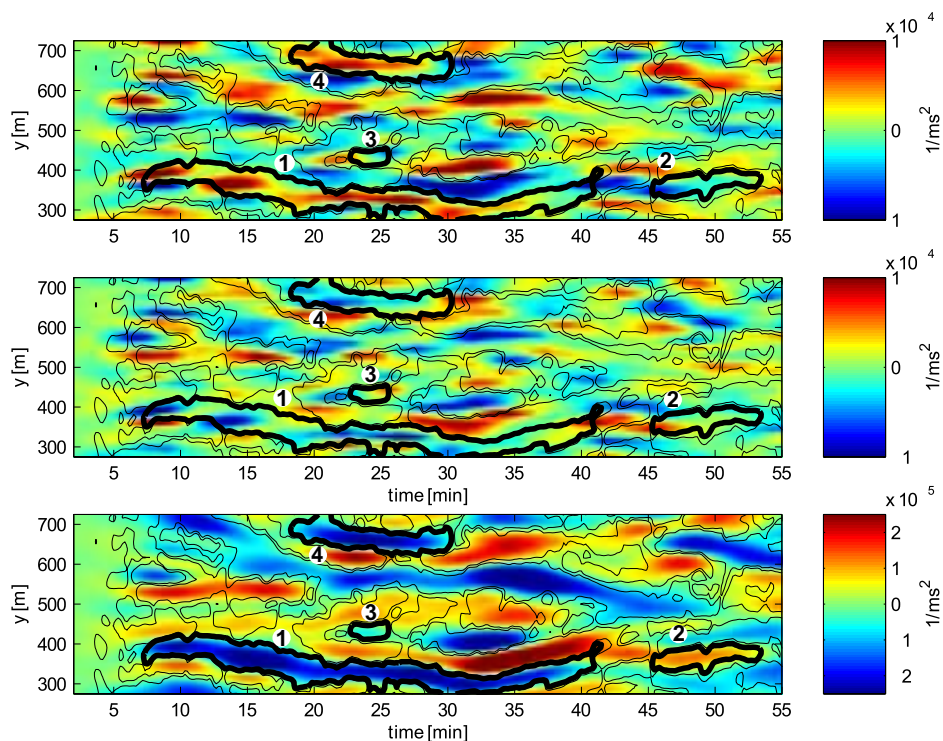


Figure 11. Normally incident random wave group sequence. (top) Time stack of low-pass-filtered ($T > 200$ s) $\frac{1}{d}\nabla_h \times \vec{\tau}_w$ at an alongshore transect taken at $x = 223$ m. (middle) A time stack of low-pass-filtered $-\frac{D_s}{Dt}$ at the same transect. (bottom) A time stack of low-pass-filtered $-\frac{1}{d}\nabla_h \times \vec{\tau}_b$. Black lines correspond to contours of $\zeta = \pm 0.002$ [$\frac{1}{ms}$] (vortex tracking threshold), and bold contours refer to vortices discussed in detail.

the water column in the opposing direction) it acts to weaken the vortex. It is important to note that this period of dissipation of potential vorticity does not necessarily mean that the vortex will no longer exist. The length of time the vortex persists is directly related to the cumulative effect of successive strengthening and weakening and is, therefore, a strong function of the sequence of wave groups incident on the beach.

[43] In this case (Figure 10e) the initiation of the vortex is associated with a strong positive stirring of the water column by the low-frequency curl of the wave forcing. This quantity remains positive for over 35 min and causes the vortex to persist for the same duration. We note that there are periods within this time history (e.g., at $t = 24$ min) where the low-frequency time series of the curls of bottom friction and wave forcing are of equal importance; however, these periods are short-lived and last only 1–2 min. The identified vortex strengthens during times of strong wave forcing and persists until the wave forcing term changes sign and causes a significant reverse stirring of the water column ($t = 40$ min). This causes a rapid dissipation of the vortex until it can no longer be identified by the vortex tracking algorithm. Interestingly, this is also the time when the vortex migrates shoreward of the bar crest (Figure 10g) where wave groupiness has been reduced because of wave breaking over the bar and wave forcing of vorticity is small because of a lack of breaking in this region. For all the vortices analyzed, we did not observe situations when the curl of the wave forcing remained small for sufficient time

such that bottom friction could become responsible for the decay and eventual demise of a vortex. Instead, vortex demise occurred when the low-frequency stirring effect of the wave forcing reversed in sign for a sufficient amount of time.

[44] In order to illustrate the range of conditions observed in the results, we show time-space plots of the terms in the low-frequency potential vorticity balance at an alongshore transect just offshore of the bar crest (Figure 11). In essence this shows point balances of the potential vorticity equation at each alongshore position for the given cross-shore transect. The contour lines outline instances when the potential vorticity is above the threshold used in the vortex tracking algorithm. Hence, these closed lines indicate the temporal and alongshore extent of an identified vortex at this cross-shore position. Although we use a nonlinear bottom friction parametrization, the curl of the bottom friction is representative of the potential vorticity. Vortex 1 (as labeled in Figure 11) is the vortex previously discussed. Vortex 3, which develops around $t = 22$ min, illustrates a situation where a vortex is generated, but exists for only approximately 5 min because the low-frequency curl of the wave forcing reverses sign (from positive to negative) soon after vortex generation and destroys the vortex. Vortices 2 and 4 exhibit the same dynamic balance between curl of the radiation stress forcing and total changes of potential vorticity and are examples of positive and negative vortical motions existing in the domain for O(10 min). Overall, vortices exist for periods of time

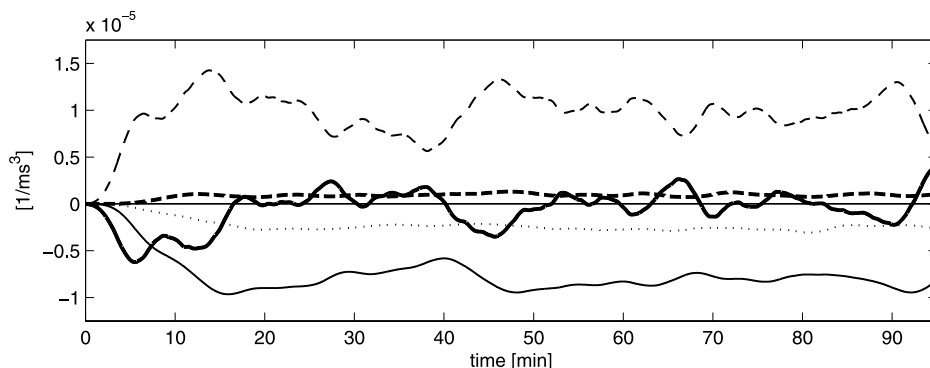


Figure 12. Random wave groups with stable alongshore mean current. Low-pass-filtered ($T > 200$ s) potential enstrophy balance integrated over all alongshore positions from the bar trough to the offshore boundary. Thick solid line, ENS_i ; thick dashed line, $PROD_{shear}$; thin dashed line, $PROD_{wave}$; dotted line, MIX ; thin solid line, $FRIC$.

ranging from 5–45 min. Their alongshore position during this time can be quite stationary, or they can migrate alongshore for distances up to 100 m.

5.2. Oblique Incidence

[45] In section 5.1 we show that under normally incident wave conditions the vortices can exist for $O(10)$ min or more because a low-frequency component of the curl of the radiation stress gradients exists. It is not clear, however if the potential vorticity balance changes when wave group-forced vortices are superimposed on an alongshore current, or if they have characteristics that can be distinguished from other low-frequency motions in the surf zone such as shear instabilities of the alongshore current. The following model simulations address these questions by considering oblique wave groups with varying degrees of groupiness coexisting with both stable and unstable alongshore currents. For these cases the model domain is $700 \text{ m} \times 2000 \text{ m}$ with a variable cross-shore resolution of 1.25–4.90 m, and an alongshore grid spacing of 7.81 m. This alongshore extent is twice that used by *Noyes et al.* [2005] in their model-data comparisons of shear instabilities and should therefore ensure that these motions are adequately resolved. We also impose periodicity at the lateral boundaries.

5.2.1. Stable Alongshore Current Profile

[46] First, we consider a situation where the mean alongshore current is expected to be stable. The mean wave height and peak period of the offshore wavefield are 1 m and 10 s, respectively (resulting in a time series with $GF = 0.6$). The peak wave angle is -8° which forces a mean alongshore current in the positive y direction. The mean alongshore current profile is obtained by averaging the alongshore velocities over the last half of the simulation and over all alongshore transects. A stability analysis of this alongshore current profile indicates stability.

[47] Time series of potential vorticity over the bar (not shown) are very similar to the balances analyzed for the normally incident random waves. The perturbation potential enstrophy balance is also similar (Figure 12) indicating the dominant role of the wave group forcing in generating and controlling the temporal variations in potential vorticity. However, in this case a shear production term is also present even though the underlying mean alongshore current is stable. This is because the alongshore current is sheared

in the cross-shore direction, hence the cross-shore gradient of the associated alongshore-averaged potential vorticity is nonzero. Coupling this with the nonzero potential enstrophy fluctuations associated with the wave group-forced vortices gives rise to a nonzero shear production term. Despite the presence of this additional source term, we note that the temporal evolution of the time rate of change of potential enstrophy still closely resembles the time variability in the wave group-forcing term. Bottom friction and momentum mixing continue to act as enstrophy sinks.

[48] In order to analyze the fate of individual vortices, time-space plots of the terms in the low-frequency potential vorticity balance at an alongshore transect just offshore of the bar crest (Figure 13) are analyzed. The time stack of the curl of the bottom friction (Figure 13, bottom) is a close proxy for a time stack of potential vorticity, and a few vortices are selected for closer examination. Once vortices are generated, they propagate in the alongshore direction. Note that the curl of the wave radiation stress gradients (Figure 13, top) does not display a propagating nature, although the waves themselves arrive obliquely. Hence, the alongshore propagation of the vortices is not dictated by the wave groups; instead, the vortices are advected by the mean background current. As a vortex is advected alongshore it encounters stirring that either strengthens or weakens it and the vortex ceases to exist only when it is affected by sufficiently strong forcing that stirs in an opposing direction.

[49] *Reniers et al.* [2004] already evaluated the frequency-wave number signature of vortices caused by normally incident wave groups. Here, we analyze the signature for obliquely incident groups by constructing the spectrum from time series of vorticity. This approach exploits the filtering of gravity motions inherent in the quantity of vorticity [*Kirby and Chen*, 2002] which is evident by the comparison of frequency-wave number spectra computed using vorticity and both components of velocity shown in Figure 14. The computed spectra have been band averaged, resulting in a frequency and wave number resolution of $df = 0.0017 \text{ Hz}$ and $dk = 0.0025 \text{ m}^{-1}$, respectively. The cross-shore and alongshore velocity spectra show the presence of gravity wave motions (e.g., edge waves) that are absent in the potential vorticity signal because these motions are irrotational. However, the signature of the wave group-

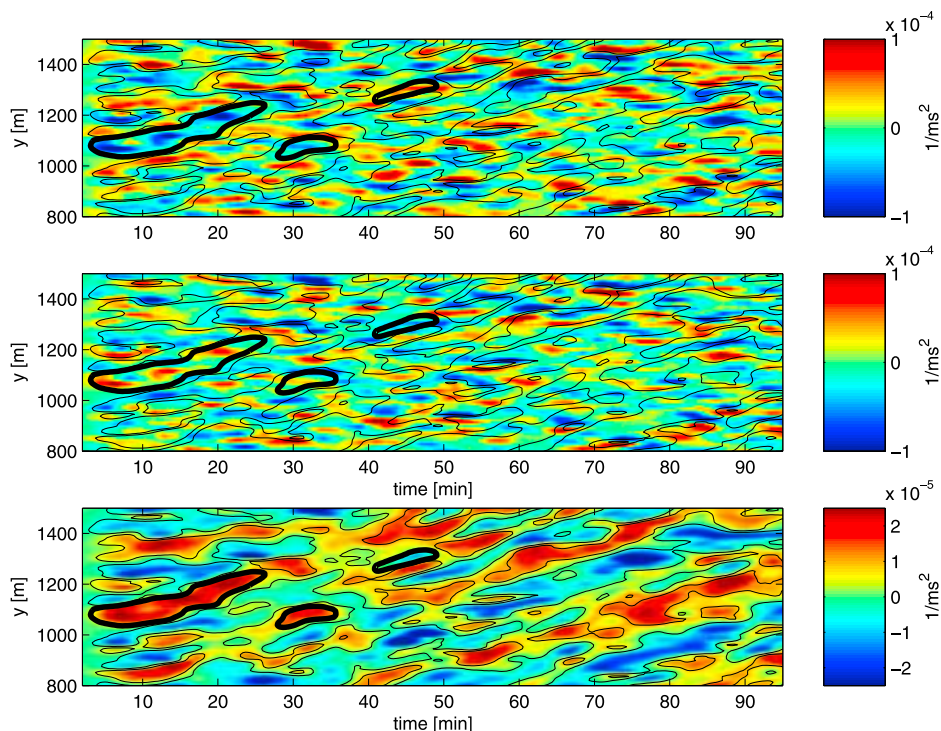


Figure 13. Random wave groups with stable alongshore mean current. (top) Time stack of low-pass-filtered ($T > 200$ s) $\frac{1}{d}\nabla_h \times \overline{\tau_w}$ at an alongshore transect taken at $x = 223$ m. (middle) A time stack of low-pass-filtered $-\frac{D\zeta}{Dt}$ at the same transect. (bottom) A time stack of low-pass-filtered $-\frac{1}{d}\nabla_h \times \overline{\tau_b}$. Black lines correspond to contours of low-pass-filtered $\zeta = \pm 0.002$ [$\frac{1}{ms}$] (vortex tracking threshold), and bold contours are shown to better highlight phenomena discussed in the text.

forced vortices is evident in all three spectra and lies along a linear ridge indicative of nondispersive alongshore propagation. Hence, while we use vorticity as a measure in this numerical study, field measurements of velocity would record the low-frequency oscillations described here. The resulting frequency–wave number spectra are similar to those measured in the presence of shear instabilities of the alongshore current, even though the alongshore current in this case is stable.

[50] We quantify the alongshore phase speed at all cross-shore locations by determining the slope of a best fit line of

the spectrum over the entire positive frequency range following *Özkan-Haller and Kirby [1999]* and compare this estimate to the mean alongshore current profile (not shown). We find that the phase speed over and seaward of the bar corresponds to the local value of the alongshore current. This is consistent with the notion that the vortices are directly forced by the wave groups and advected alongshore by the mean alongshore current. Any differences in the phase speed and mean alongshore current velocities are likely due to several factors. For example, the advection speed is likely affected by mutual interactions with neigh-

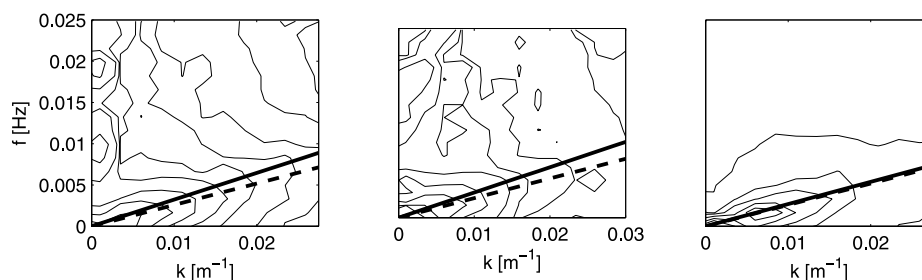


Figure 14. Random wave groups with stable alongshore mean current. The frequency–wave number spectrum of (left) cross-shore velocity and (middle) alongshore velocity at $x = 223$ m with contour levels corresponding to [10, 30, 100, 300, 1000, 3000, 10,000, 30,000, 100,000] ($m^3 s^{-1}$). (right) The frequency–wave number spectrum of vorticity with contour levels [1, 10, 25, 50, 75, 100, 250, 500, 750, 1000, 10,000] ($m^{-1} s^{-1}$). Only the half of the spectrum corresponding to the direction of mean alongshore current is shown. The estimated best fit dispersion line (solid line) and local mean alongshore current (dashed line) are also shown.

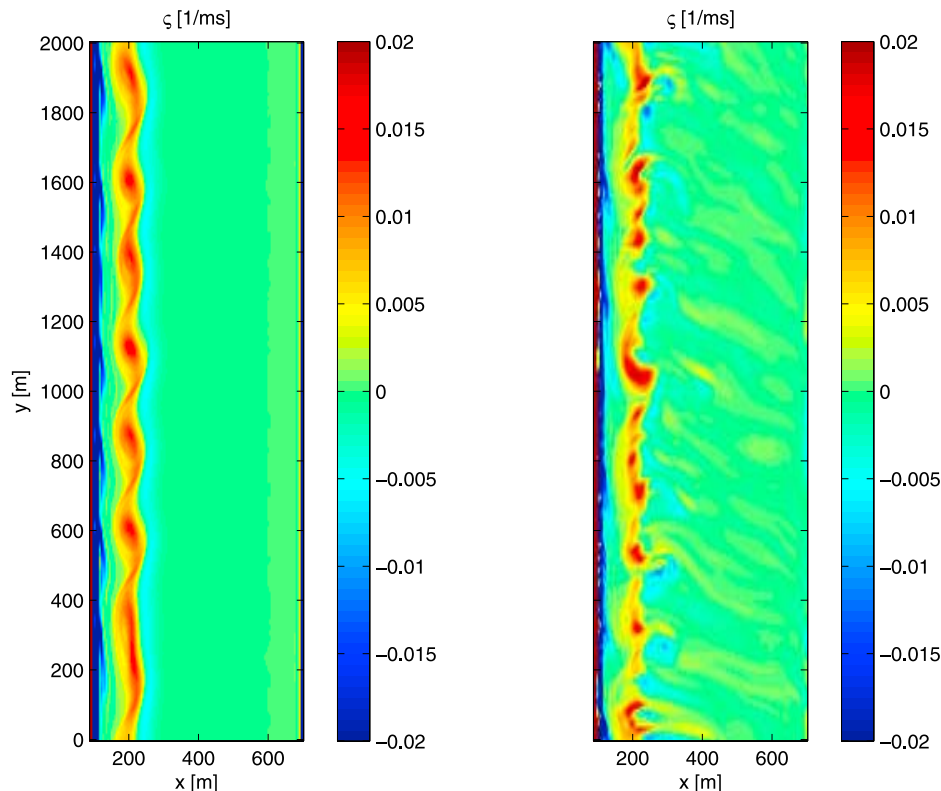


Figure 15. Oblique random wave group sequence. Snapshots of the vorticity field in two cases: (left) no offshore wave groups and (right) a wavefield with the same offshore peak characteristics ($H_{mean} = 1$ m, $T_p = 10$ s, $\theta = -20^\circ$) and an offshore groupiness factor of $GF = 0.6$. The snapshot is taken at $t = 75$ min.

boring vortices and self-interaction processes due to the barred bathymetry as discussed in detail by *Kennedy et al.* [2006]. These results suggest that when wave group vortices coexist with a stable alongshore current, the temporal variability of the vortices is once again controlled by the curl of the wave forcing, and advection by the mean flow dominates vortex transport.

5.2.2. Unstable Alongshore Current Profile

[51] A larger angle of incidence of -20° results in a stronger alongshore current that is moderately unstable. For these cases the mean wave height of the group time series is 1 m and wave period remains at 10 s. If no groupiness is included, the resulting vorticity field (Figure 15) shows the characteristics of a fluctuating eddy regime identified by *Slinn et al.* [1998]. The length scale associated with the shear instabilities is 265 m, and the propagation speed is 35 cm s^{-1} . The inclusion of groupiness ($GF = 0.6$) results in a vorticity field with similar length scales, although the vortices are not as well defined and variability at smaller length scales is evident (Figure 15). We note that the simulation using a steady wavefield (no groups) is forced using the mean forcing associated with the simulation including wave groups. This ensures that the mean quantities associated with the momentum balances of both simulations are consistent. Time series of the potential vorticity balance computed at a single point just seaward of the bar crest (Figure 16) highlight the different dynamics associated with the two cases. When groups are not present (Figure 16, top), the curl of the wave forcing is approximately constant

because of the lack of alongshore wave variations; however, very minor oscillations develop because of small changes in the total water depth caused by the shear waves. Prior to the development of the shear waves ($t = 30$ min), the wave forcing is balanced primarily by the lateral mixing and bottom friction. A balance computed close to the peak in the alongshore current profile rather than offshore of the bar crest shows a dominant balance between the wave forcing and bottom friction as is traditionally expected. However, because the location of this point balance is further offshore, mixing is the dominant process responsible for spreading the alongshore current profile to this cross-shore position. After the shear waves have developed, temporal variations in the local changes of potential vorticity are mainly balanced by the variations in the advective changes of potential vorticity. Any local imbalance between these two terms is the total time derivative of potential vorticity, and it is balanced by the curl of the bottom friction. This is true for all cross-shore positions from the bar trough to offshore of the bar crest and is characteristic of a free motion as previously discussed. The potential enstrophy balance (Figure 17, top) confirms that shear production is the primary source of enstrophy and, after some initial adjustment, the time rate of change of enstrophy remains zero.

[52] In contrast, when wave groups are included, temporal variations in the material derivative of vorticity (Figure 16, bottom) are balanced by the curl of the wave forcing rather than the bottom friction. Separation of the total time derivative into local and advective components reveals that

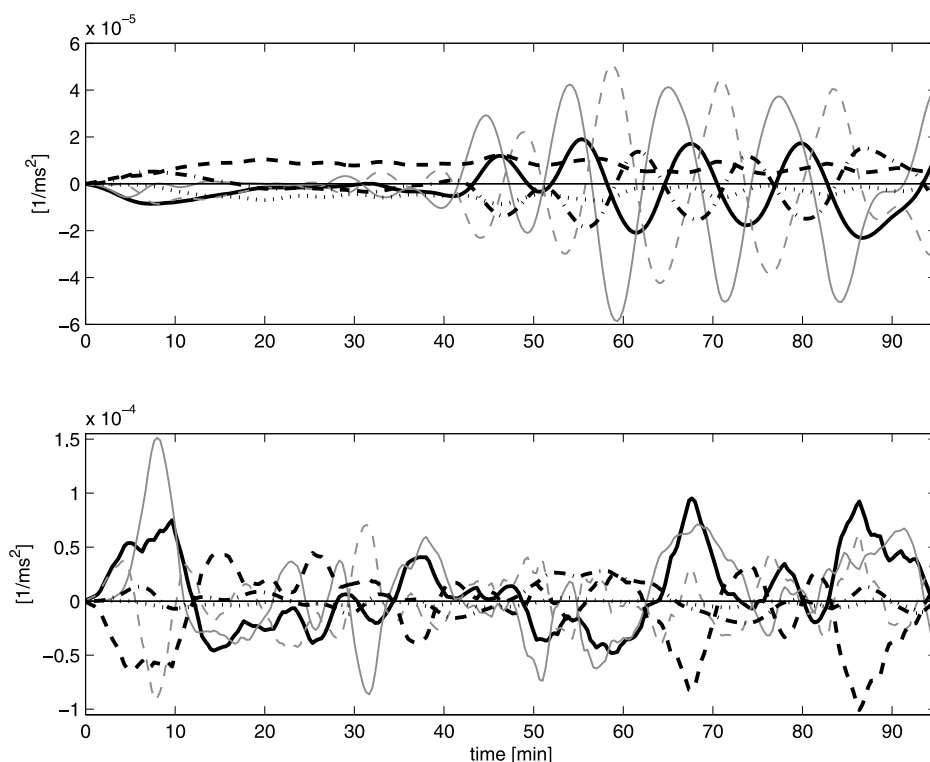


Figure 16. Random wave groups with unstable alongshore mean current. Low-pass-filtered ($T > 200$ s) potential vorticity balance for oblique incident waves ($H_{mean} = 1$ m, $T_p = 10$ s, $\theta = -20^\circ$) (top) without wave groups ($GF = 0$) and (bottom) with $GF = 0.6$. Black solid line, $-\frac{D_s}{Dt}$; gray dashed line, $-\frac{\partial s}{\partial t}$; gray solid line, $-(u\frac{\partial s}{\partial x} + v\frac{\partial s}{\partial y})$; black dashed line, $\frac{1}{d}\nabla_h \times \overline{\tau_w}$; black dash-dotted line, $-\frac{1}{d}\nabla_h \times \overline{\tau_b}$. Both balances computed at $x = 223$ m and $y = 344$ m.

the magnitudes of these terms are now larger than the total derivative. This is in contrast to all the wave group cases analyzed so far where the magnitude of the total derivative formed a general upper bound for the local and advective terms. The enstrophy balance (Figure 17, bottom) confirms that in addition to wave forcing, shear production plays an important role in generating vorticity which can explain the increased prominence of the local and advective effects. Further, we find that the time rate of change of enstrophy over the entire domain varies significantly in time, and these fluctuations mimic the variability in the wave forcing. This indicates that the temporal behavior of the vortices is dictated by the wave forcing even in a situation where half of the vorticity is generated by an instability process. The turbulent mixing component and the bottom shear stress remain as important dissipative quantities.

[53] We note here, that the vorticity and enstrophy balances in the presence of wave grouping revert back to the free balance in the bar trough, where waves are not breaking and no wave forcing is present. Near the shoreline, however, when waves begin to break again, the balance is the same as that shown in this analysis.

[54] We also show the frequency–wave number spectrum of alongshore velocity and potential vorticity for both cases at a transect just seaward of the bar ($x = 223$ m) in Figure 18. The local mean alongshore current and the alongshore phase speed of the vortical motions are also shown. Note that for the case where groups are considered, increased mixing

occurs which broadens the mean alongshore current profile. This broadening reduces the peak magnitude of the alongshore current as indicated by the difference in local mean alongshore current speed (slope of dashed lines) shown in Figure 18. Interestingly, including wave group variations causes a substantial broadening of the frequency–wave number spectrum. This offers an explanation for why the shapes of modeled spectra in previous research have consistently been much narrower than observed in the field. Our findings suggest that accounting for wave group forcing may improve data-model comparisons.

[55] Finally, we examine the effect of incrementally decreasing the amount of groupiness present in the offshore wave conditions. We construct two additional time series ($GF = 0.3$ and $GF = 0.1$) that contain exactly the same set of groups; however, the magnitude of the spatial and temporal gradients of radiation stress gradients are adjusted, while maintaining the same mean quantities. Not surprisingly, in simulations where the amount of wave groupiness is decreased, the contribution of enstrophy production from the perturbation wavefield is less important and the production by the shear in the mean alongshore current dominates. However, the temporal variability in the wave forcing still affects the time rate of change of enstrophy. To assess the effect on the width of the frequency–wave number spectra, we compute the half-power bandwidth of the frequency spectrum of potential vorticity (integrated over all wave numbers) at each cross-shore location for each case (Figure 19). Note

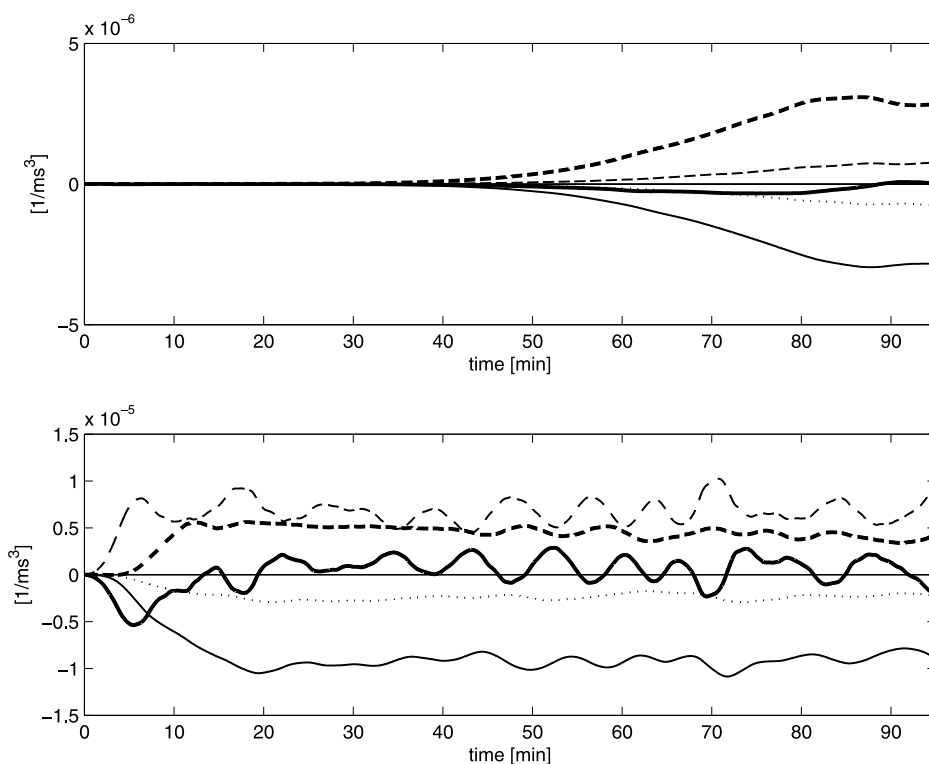


Figure 17. Random wave groups with unstable alongshore mean current. Low-pass-filtered ($T > 200$ s) potential enstrophy balance integrated over all alongshore positions from the bar trough to the offshore boundary for oblique incident waves ($H_{mean} = 1$ m, $T_p = 10$ s, $\theta = -20^\circ$) (top) without wave groups ($GF = 0$) and (bottom) with $GF = 0.6$. Thick solid line, ENS ; thick dashed line, $PROD_{shear}$; thin dashed line, $PROD_{wave}$; dotted line, MIX ; thin solid line, $FRIC$.

that estimates of the frequency–wave number spectrum offshore of the surf zone contain significantly less energy and are not entirely meaningful. We find that as the groupiness decreases, the broadness of the frequency–wave number spectrum just seaward of the bar ($x \approx 250$ m) also decreases. Wave breaking over the bar crest reduces the amount of groupiness in all of the time series (large waves break, while adjacent small waves do not) and from the bar crest shoreward, the spectral width does not vary between the time series.

6. Summary and Conclusions

[56] In this study, the temporal response of wave group induced vortices on an alongshore uniform barred beach was evaluated using both simplified and realistic random wave conditions. The persistence of the vortices was investigated to determine the mechanism by which they can continue to exist over many wave group periods. We utilized a vortex tracking algorithm used in the study of 2-D turbulence to follow the evolution of individual vortices and also evaluated the vorticity balance at fixed locations.

[57] For both normally and obliquely incident waves, the temporal variations in the total derivative of potential vorticity are dictated by the curl of the radiation stress forcing. The latter quantity characterizes the ability of the wavefield to “stir” the fluid in a particular direction. We find that low-frequency modulations in the curl of the wave

forcing are responsible for dictating the lifespan of a particular vortex. Given this strong control by the wave forcing, wave group vortices over the bar are generally not free motions that decay in time because of the effects of friction, as previously suggested. Instead, once generated, the temporal evolution of an individual vortex is dictated by all subsequent rotational forcing contributions it experiences because of breaking waves, with the vortex gaining and losing strength depending on the sign of such “stirring.” Hence, a vortex persists until wave forcing of the opposite sign decelerates it for a sufficient time. Therefore, the exact sequencing of the wave groups controls the life span of any vortex. In the simulations carried out here, vortices exhibited lifespans between 5–45 min. Bottom friction, while an important component, does not control the temporal variability in potential vorticity or lead to the demise of individual vortices located on top of and seaward of the bar crest. Free motions are instead only observed during brief periods when wave forcing is weak. In the bar trough, however, we find that the total time rate of change of potential vorticity in the model is balanced primarily by bottom friction because waves are not breaking and therefore wave forcing is absent.

[58] We also evaluated the low-frequency spectral signature of the wave group–forced vortices when waves were obliquely incident and a mean alongshore current was present. In situations where this alongshore current is stable, we find that energy due to these vorticity motions occupies

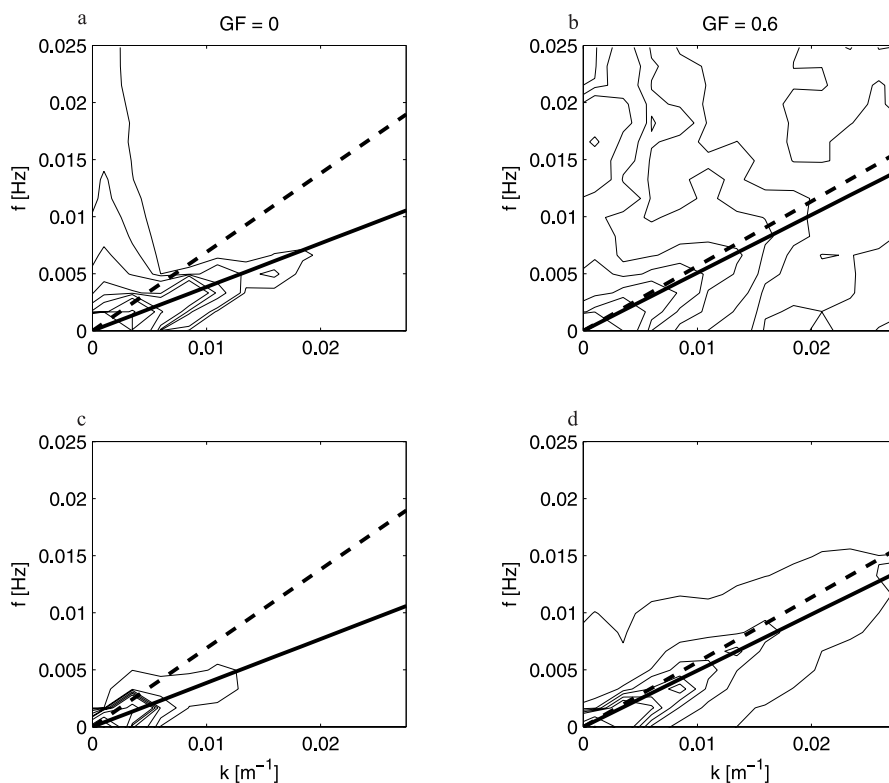


Figure 18. Random wave groups with unstable alongshore mean current. Frequency–wave number spectra of (a, b) alongshore velocity and (c, d) vorticity for the alongshore transect at $x = 223$ m. Offshore wave time series with no wave group variations (Figures 18a and 18c) and with $GF = 0.6$ (Figures 18b and 18d) are shown. Both cases have an offshore wave angle of -20° , mean wave height of 1 m, and 10 s peak period. Contour levels of [10, 30, 100, 300, 1000, 3000, 10,000, 30,000, 100,000] ($\text{m}^3 \text{s}^{-1}$) are given for velocity spectra, and contour levels of [1, 10, 25, 50, 75, 100, 250, 500, 750, 1000, 10,000] ($\text{m}^{-1} \text{s}^{-1}$) are shown for vorticity. In all cases, only the half of the spectrum corresponding to the direction of mean alongshore current is shown. The estimated vortex phase speed (solid line) and modeled local mean alongshore current (dashed line) are given.

a ridge in the frequency–wave number spectrum, very similar to the spectral signal of instabilities of the alongshore current. The potential enstrophy (vorticity squared) balance clearly elucidates that the perturbations in the curl of the wave forcing (i.e., wave groups) are the dominant

mechanism in the production of enstrophy. Previous observations of low-frequency energy during conditions where the current is linearly stable have so far gone largely unexplained (see, for instance, observations at Leadbetter Beach, California, summarized by *Dodd et al.* [1992]). We

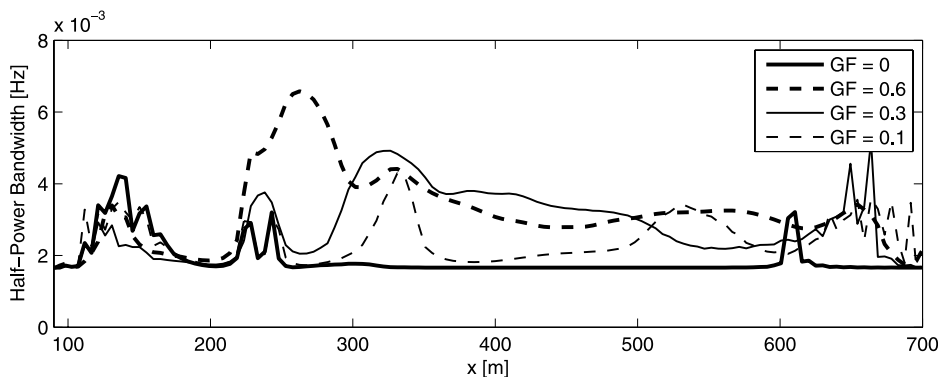


Figure 19. Unstable alongshore mean current. Half-power bandwidth of the frequency–wave number spectra of potential vorticity (integrated over all wave numbers) versus cross-shore distance for $GF = 0$ (thick solid line), $GF = 0.1$ (thin dashed line), $GF = 0.3$ (thin solid line), and $GF = 0.6$ (thick dashed line).

suggest here that such energy may be due to the presence of a groupy wave train and the advection of resulting wave group-forced vortices by the mean alongshore current.

[59] If the alongshore current is unstable, we find that the shear instabilities and wave group-forced vortices occupy the same range in the frequency-wave number spectrum. However, when wave groupiness is accounted for, the frequency-wave number spectrum displays a much broader ridge, especially over and seaward of the bar crest. The level of broadness is increased with the level of groupiness in the wave height time series. In the bar trough, where groupiness is reduced because of wave breaking over the bar, this broadening effect is suppressed. In light of the fact that previous model simulations of shear instabilities [e.g., Özkan-Haller and Kirby, 1999; Noyes et al., 2005] generally produce spectra that are often too narrow when compared to observed spectra, our finding suggests that spectral model-data comparisons may be improved if wave grouping is taken into account.

[60] The balance of potential enstrophy in the domain confirms the role that wave groups have in generating vortical motions in the surf zone. We find that potential enstrophy production due to wave grouping is the sole source of vorticity in the domain for normally incident waves, the primary source for obliquely incident waves in the presence of a stable alongshore current, and an important component (along with shear production) when an unstable alongshore current is present. For the case of an unstable alongshore current, as the amount of groupiness in the domain increases, the production of enstrophy due to wave groups becomes equally as important as the production due to the shear in the mean alongshore current. While previous observations of vorticity motions in the presence of oblique waves have so far been interpreted exclusively as shear instabilities, these findings suggest that a significant portion of this energy may be directly forced by wave groups.

[61] **Acknowledgments.** The authors thank three anonymous reviewers for their constructive comments and suggestions. We also thank Steve Henderson, Merrick Haller, and Rob Holman for insightful discussions throughout this study. This research is sponsored by the Office of Naval Research's Coastal Geosciences Program under grants N00014-02-1-0198 and N00014-07-1-0852.

References

- Allen, J. S., P. A. Newberger, and R. A. Holman (1996), Nonlinear shear instabilities of alongshore currents on plane beaches, *J. Fluid Mech.*, *310*, 181–213, doi:10.1017/S0022112096001772.
- Battjes, J. A. (1975), Modeling of turbulence in the surf zone, in *Symposium on Modeling Techniques: 2nd Annual Symposium of the Waterways, Harbors, and Coastal Engineering Division of ASCE*, vol. 2, pp. 1050–1061, Am. Soc. of Civ. Eng., New York.
- Battjes, J. A., and J. P. F. M. Janssen (1978), Energy loss and set-up due to breaking random waves, in *Coastal Engineering (1978 Germany): Proceedings of Sixteenth Coastal Engineering Conference*, pp. 68–81, Am. Soc. of Civ. Eng., New York.
- Bouws, E., H. Gunther, W. Rosenthal, and C. Vincent (1985), Similarity of the wind wave spectrum in finite water depth, *J. Geophys. Res.*, *90*, 975–986.
- Brocchini, M., A. Kennedy, L. Soldini, and A. Mancinelli (2004), Topographically controlled, breaking-wave-induced macrovortices. Part 1. Widely separated breakwaters, *J. Fluid Mech.*, *507*, 289–307, doi:10.1017/S002211200400878X.
- Bühler, O., and T. E. Jacobson (2001), Wave-driven currents and vortex dynamics on barred beaches, *J. Fluid Mech.*, *449*, 313–339, doi:10.1017/S0022112001006322.

- Dodd, N., and E. B. Thornton (1990), Growth and energetic of shear waves in the nearshore, *J. Geophys. Res.*, *95*, 16,075–16,083.
- Dodd, N., J. Oltman-Shay, and E. Thornton (1992), Shear instabilities in the longshore current: A comparison of observation and theory, *J. Phys. Oceanogr.*, *22*, 62–82, doi:10.1175/1520-0485(1992)022<0062:SIITLC>2.0.CO;2.
- Garcez Faria, A. F. G., E. B. Thornton, T. P. Stanton, C. V. Soares, and T. C. Lippmann (1998), Vertical profiles of longshore currents and related bed shear stress and bottom roughness, *J. Geophys. Res.*, *103*, 3217–3232.
- Feddersen, F., R. T. Guza, S. Elgar, and T. Herbers (2000), Velocity moments in alongshore bottom stress parameterizations, *J. Geophys. Res.*, *105*, 8673–8686.
- Fowler, R. E., and R. A. Dalrymple (1990), Wave group forced nearshore circulation, in *Coastal Engineering (1990): Symposium on Modeling Techniques, Waterway, Harbors and Coastal Engineering Division of ASCE*, edited by B. L. Edge, pp. 729–742, Am. Soc. of Civ. Eng., New York.
- Haller, M. C., U. Putrevu, J. Oltman-Shay, and R. A. Dalrymple (1999), Wave group forcing of low frequency surf zone motion, *Coastal Eng. J.*, *41*, 121–136.
- Haller, M. C., R. A. Dalrymple, and I. A. Svendsen (2002), Experimental study of nearshore dynamics on a barred beach with rip channels, *J. Geophys. Res.*, *107*(C6), 3061, doi:10.1029/2001JC000955.
- Johnson, D., and C. Pattiaratchi (2004), Transient rip currents and nearshore circulation on a swell-dominated beach, *J. Geophys. Res.*, *109*, C02026, doi:10.1029/2003JC001798.
- Johnson, D., and C. Pattiaratchi (2006), Boussinesq modelling of transient rip currents, *Coastal Eng.*, *53*, 419–439, doi:10.1016/j.coastaleng.2005.11.005.
- Kennedy, A., M. Brocchini, L. Soldini, and E. Gutierrez (2006), Topographically controlled, breaking-wave-induced macrovortices. Part 2. Changing geometries, *J. Fluid Mech.*, *559*, 57–80, doi:10.1017/S0022112006009979.
- Kirby, J. T., and Q. Chen (2002), Examining the low frequency predictions of a Boussinesq wave model, in *Coastal Engineering 2002: Proceedings of the 28th International Conference*, edited by J. McKee Smith, pp. 1075–1087, Am. Soc. of Civ. Eng., Reston, Va.
- List, J. (1991), Wave groupiness in the nearshore, *Coastal Eng.*, *14*, 475–496, doi:10.1016/0378-3839(91)90024-B.
- Longuet-Higgins, M. S., and R. Stewart (1964), Radiation stresses in water waves; A physical discussion with applications, *Deep Sea Res. Oceanogr. Abstr.*, *11*, 529–562.
- MacMahan, J. H., E. B. Thornton, T. P. Stanton, and A. J. Reniers (2005), Ripex: Observations of a rip current system, *Mar. Geol.*, *218*(1–4), 113–134, doi:10.1016/j.margeo.2005.03.019.
- McWilliams, J. C. (1990), The vortices of two-dimensional turbulence, *J. Fluid Mech.*, *219*, 361–385, doi:10.1017/S0022112090002981.
- Noyes, T. J., R. T. Guza, F. Feddersen, S. Elgar, and T. H. C. Herbers (2005), Model-data comparisons of shear waves in the nearshore, *J. Geophys. Res.*, *110*, C05019, doi:10.1029/2004JC002541.
- Özkan-Haller, H. T., and J. T. Kirby (1999), Nonlinear evolution of shear instabilities of the longshore current: A comparison of observations and computations, *J. Geophys. Res.*, *104*, 25,953–25,984.
- Özkan-Haller, H., and Y. Li (2003), Effects of wave-current interaction on shear instabilities of longshore currents, *J. Geophys. Res.*, *108*(C5), 3139, doi:10.1029/2001JC001287.
- Peregrine, D. (1998), Surf zone currents, *Theor. Comput. Fluid Dyn.*, *10*(1), 295–309, doi:10.1007/s001620050065.
- Reniers, A. J. H. M., J. A. Roelvink, and E. B. Thornton (2004), Morphodynamic modeling of an embayed beach under wave group forcing, *J. Geophys. Res.*, *109*, C01030, doi:10.1029/2002JC001586.
- Reniers, A. J. H. M., J. MacMahan, E. B. Thornton, and T. P. Stanton (2007), Modeling of very low frequency motions during RIPEX, *J. Geophys. Res.*, *112*, C07013, doi:10.1029/2005JC003122.
- Roelvink, J. A. (1993), Dissipation in random wave groups incident on a beach, *Coastal Eng.*, *19*, 127–150.
- Ryrie, S. (1983), Longshore motion due to obliquely incident wave group, *J. Fluid Mech.*, *137*, 273–284.
- Sleath, J. F. A. (1984), *Sea Bed Mechanics*, vol. 24, *Adv. Ser. Ocean Eng.*, vol. 24, John Wiley, New York.
- Slinn, D., J. Allen, P. Newberger, and R. Holman (1998), Nonlinear shear instabilities of alongshore currents over barred beaches, *J. Geophys. Res.*, *103*, 18,357–18,379.
- Spydell, M., and F. Feddersen (2009), Lagrangian drifter dispersion in the surf zone: Directionally spread normally incident waves, *J. Phys. Oceanogr.*, *39*, 809–830.
- Spydell, M., F. Feddersen, R. Guza, and W. Schmidt (2007), Observing surf-zone dispersion with drifters, *J. Phys. Oceanogr.*, *37*, 2920–2939.

- Terrile, E., R. Briganti, M. Brocchini, and J. Kirby (2006), Topographically-induced enstrophy production/dissipation in coastal models, *Phys. Fluids*, *18*, 126603, doi:10.1063/1.2400076.
- Thornton, E. B., and R. T. Guza (1983), Transformation of wave height distribution, *J. Geophys. Res.*, *88*, 5925–5938.
- Van Dongeren, A., A. Reniers, and J. Battjes (2003), Numerical modeling of infragravity wave response during DELILAH, *J. Geophys. Res.*, *108*(C9), 3288, doi:10.1029/2002JC001332.
- Wright, D., and K. Thompson (1983), Time-averaged forms of the nonlinear stress law, *J. Phys. Oceanogr.*, *13*, 341–346, doi:10.1175/1520-0485(1983)013<0341:TAFOTN>2.0.CO;2.
- Zhao, Q., I. A. Svendsen, and K. Haas (2003), Three-dimensional effects in shear waves, *J. Geophys. Res.*, *108*(C8), 3270, doi:10.1029/2002JC001306.

J. W. Long and H. T. Özkan-Haller, College of Oceanic and Atmospheric Sciences, Oregon State University, 104 Ocean Administration Building, Corvallis, OR 97331-5503, USA. (jlong@coas.oregonstate.edu)